The influence of winter water on phytoplankton blooms in the Chukchi Sea

Kate E. Lowry*[1], Robert S. Pickart[2], Matthew M. Mills[1], Zachary W. Brown[1], Gert L. van Dijken[1], Nicholas R. Bates[3], Kevin R. Arrigo[1]

[1]Department of Environmental Earth System Science, Stanford University, Stanford, CA 94305, USA

[2]Woods Hole Oceanographic Institution, Woods Hole, MA 02540, USA

[3]Bermuda Institute of Ocean Sciences, St. Georges, Bermuda

* Corresponding Author: lowryk@stanford.edu, 1-650-736-0688

Abstract

The flow of nutrient-rich winter water (WW) through the Chukchi Sea plays an important and previously uncharacterized role in sustaining summer phytoplankton blooms. Using hydrographic and biogeochemical data collected as part of the ICESCAPE program (June-July 2010-11), we examined phytoplankton bloom dynamics in relation to the distribution and circulation of WW (defined as water with potential temperature ≤ -1.6°C) across the Chukchi shelf. Characterized by high concentrations of nitrate (mean: 12.3 ± 5.13 μmol L^{-1}) that typically limits primary production in this region, WW was correlated with extremely high phytoplankton biomass, with mean chlorophyll *a* concentrations that were three-fold higher in WW (8.64 ± 9.75 μg L^{-1}) than in adjacent warmer water (2.79 ± 5.58 μg L^{-1}). Maximum chlorophyll *a* concentrations (~30 μg L^{-1}) were typically positioned at the interface between nutrient-rich WW and shallower, warmer water with more light availability. Comparing satellite-based calculations of open water duration to phytoplankton biomass, nutrient concentrations, and oxygen saturation revealed widespread evidence of under-ice blooms prior to our sampling, with biogeochemical properties indicating that blooms had already terminated in many places where WW was no longer present. Our results suggest that summer phytoplankton blooms are

sustained for a longer duration along the pathways of nutrient-rich WW and that biological hotspots in this region (e.g. the mouth of Barrow Canyon) are largely driven by the flow and confluence of these extremely productive pathways of WW that flow across the Chukchi shelf.

Key Words: phytoplankton, winter water, under-ice blooms, biological hotspots, Chukchi Sea

1. Introduction

Located north of the Bering Strait between Alaska and Far East Russia, the Chukchi Sea is the gateway of the Pacific Ocean to the Arctic. With a total area of 620,000 km^2 and a median depth of approximately 50 m (Jakobsson, 2002), the Chukchi Sea contains a wide and shallow continental shelf that comprises 10% of the total Arctic Ocean shelf area (Jakobsson et al., 2004; Carmack and Wassman, 2006). The importance of the Chukchi Sea as an inflow shelf sea (Carmack and Wassmann, 2006) that ventilates the upper halocline of the Arctic Ocean (Woodgate and Aagaard, 2005b; Woodgate et al., 2005a) motivates a thorough understanding of the physical and biogeochemical processes that modify Pacific-origin water masses as they transit the shelf en route to the basin.

The Chukchi Sea is a region of intense summer biological activity with a rich benthic community that supports abundant populations of marine mammals and seabirds (Loeng et al., 2005; Dunton et al., 2005; Grebmeier et al., 2006). In recent decades, the Arctic Ocean has experienced unprecedented reductions in sea ice cover and thickness (Kwok and Rothrock, 2009; Serreze et al., 2007; Stroeve et al., 2011), accompanied by an increased heat and freshwater flux through the Bering Strait (Woodgate et al., 2012). The impacts of these changes on the global carbon cycle (Bates et al., 2011) and the marine ecosystem of the Chukchi Sea (Grebmeier, 2012) are only beginning to be understood. Of particular interest is how the primary producers that form the base of the food web are being affected by the pronounced changes in the physical environment. Previous work suggests that phytoplankton are already responding to reduced sea ice cover and thickness, with evidence for increased primary production in open water (Arrigo and Van Dijken, 2011) and beneath the thinning sea ice cover (Arrigo et al., 2012, 2014; Palmer et al., 2013, 2014; Lowry et al., 2014). To fully comprehend the significance of these changes, it is necessary to further our understanding of bloom dynamics in this region.

Pacific-origin water flows northward through the Bering Strait due to the sea surface height differential resulting from the salinity difference between the Arctic and Pacific Oceans (Coachman et al., 1975). Upon entering the Chukchi Sea, the flow is steered primarily by shelf

60 bathymetry into three branches, which to some degree are distinguished by water mass properties
61 set within the Bering Sea (Coachman et al., 1975; Overland and Roach, 1987; Weingartner et al.,
62 2005). Differences in temperature, salinity (S), and nutrient concentrations between these
63 pathways result in significant variations in biogeochemical properties across the shelf (Walsh et
64 al., 1989; Cooper et al., 1997; Codispoti et al., 2005, 2013). In summertime, the easternmost
65 pathway advects Alaskan Coastal Water, which is relatively warm (>2°C), fresh (S<32), and
66 nutrient-poor (pre-bloom NO_3^- <10 μmol L^{-1}) due to the input of river runoff and the biological
67 utilization of nutrients in the eastern Bering Sea. The middle flow branch, which progresses
68 through the Central Channel between Hanna and Herald Shoals, consists largely of colder and
69 saltier Bering Shelf Water (BSW) with moderate nutrient concentrations (pre-bloom NO_3^- >10
70 μmol L^{-1}). The westernmost branch follows Hope Valley into Herald Canyon and transports a
71 large amount of Anadyr Water (AW), which is the saltiest of the three Chukchi Sea water masses
72 and has the highest nutrient concentration (pre-bloom NO_3^- > 15 μmol L^{-1}), owing to the
73 upwelling of nutrient-rich waters in the Northern Bering Sea (Hansell et al., 1993; Lee et al.,
74 2007). The precise division of transport between the branches is currently unknown. Using
75 relatively sparse mooring data, Woodgate et al. (2005b) estimated a roughly even split between
76 the branches, but recent shipboard surveys suggest that, in summer, the majority of the flow is
77 contained in the two eastern branches (Gong and Pickart, this issue; Itoh et al., 2015).
78 The water mass properties in the Chukchi Sea are heavily influenced by the seasonal cycle of
79 sea ice, both locally on the Chukchi shelf and to the south in the Bering Sea. In the winter, sea
80 ice formation causes brine rejection that can mix the entire water column and cool it to the
81 freezing point (approximately -1.9°C) (e.g. Woodgate et al., 2005b). When the convection
82 reaches the bottom it suspends regenerated nutrients from the sediments into the water column.
83 The resulting water mass, known as winter water (WW), is cold, dense, and high in nutrients.
84 The water so formed in the Bering Sea flows northward through Bering Strait during the winter
85 months and into the spring (Woodgate et al., 2005b). However, the occurrence of leads and

polynyas on the Chukchi shelf during the winter can lead to further re-freezing and the formation of "hyper-saline" WW (Weingartner et al., 1998; Itoh et al., 2012).

Although there are few winter and spring measurements in the Chukchi Sea, modeling results (Zhang et al., 2010) and field studies (e.g. Codispoti et al., 2005) indicate that surface waters are nutrient-replete in the Chukchi Sea, with NO_3^- concentrations as high as 10-20 μmol L^{-1} in non-coastal shelf waters. As sea ice retreats in the summer, the water column becomes re-stratified as surface waters freshen and warm due to a combination of ice melt, solar heating, and the influx of Pacific summer waters from the Bering Sea (Woodgate and Aagaard, 2005a; Gong and Pickart, this issue). The WW remaining on the Chukchi shelf is gradually modified by mixing with these waters and/or by direct solar heating (Weingartner et al., 2005; Gong and Pickart, 2012). As a result, the presence of WW on the shelf in summer is spatially variable, with residence times determined by the bathymetry and circulation of the Chukchi Sea (Pickart et al., submitted). By the end of summer, all of the WW gets flushed from the shelf, largely through Herald Canyon in the west (Pickart et al., 2010) and Barrow Canyon in the east (Pickart et al., 2005; Woodgate et al., 2005b; Itoh et al., 2005).

The high nutrient content and persistence of WW on the Chukchi shelf through the spring and summer suggests that this water mass plays an important, yet previously uncharacterized, role in influencing phytoplankton blooms. In this study, we examine the relationship between the early-summer hydrographic conditions in the Chukchi Sea and the phytoplankton blooms that occur on the shelf, with specific focus on the role of the nutrient-rich WW in initiating and sustaining phytoplankton blooms both before and after sea ice retreat. We assess the biological significance of WW in the summer as it drains across the Chukchi shelf by relating the location of WW to biogeochemical properties such as phytoplankton biomass, oxygen (O_2) saturation, and concentrations of nutrients and dissolved inorganic carbon (DIC). To fully elucidate the relationship between WW and phytoplankton blooms in this seasonally ice-free ecosystem, we incorporate field results from both under the sea ice and in open water, and use satellite imagery of sea ice to provide further environmental context.

2. Methods

2.1. Study region

As part of the NASA-funded Impacts of Climate on EcoSystems and Chemistry of the Arctic Pacific Environment (ICESCAPE) program, two field campaigns were carried out in the Chukchi Sea aboard USCGC *Healy*, from 18 June to 16 July 2010 (HLY1001) and from 28 June to 24 July 2011 (HLY1101). The present analysis focuses on the continental shelf of the northeastern Chukchi Sea, using data from seven transects that together span the shallow shelf waters of this region (Fig. 1). Six of the seven transects considered here were occupied in 2011, while the southernmost transect (the Central Channel line) was sampled in 2010. The Chukchi North and Hanna Shoal North transects were occupied on both cruises, providing an opportunity to compare hydrographic conditions between 2010 and 2011. Except where otherwise noted, data presented for these two transects were collected in 2011 when the sampling was more comprehensive.

2.2. Field methods and laboratory analysis

Shipboard sampling. Vertical profiles of temperature, salinity, dissolved O_2, fluorescence, and photosynthetically active radiation (PAR) were obtained approximately every 15 km using a Sea-Bird 911+ conductivity-temperature-depth instrument (CTD) with an SBE43 O_2 sensor (Sea-Bird Electronics), a fluorometer (AQIII, Chelsea Technologies Group, Ltd.), and a PAR sensor (QSP2300, Biospherical Instruments, Inc.). The CTD system was mounted on a rosette with twelve 30-liter Niskin bottles. Water samples were collected at a set of standard depths (5, 10, 25, 50, 75, 100, 150, and 200 m), and also at the depth of the fluorescence maximum and near the bottom (typically within 2-5 m of the seafloor). Most of the stations were occupied on the shelf and hence were shallower than 60 m. The temperature and conductivity sensors were calibrated pre- and post-cruise at Sea-Bird Electronics, and the conductivity sensor was also calibrated during the cruise using the deepest water sample salinity data. Based on this

information, the estimated accuracies are 0.008°C for temperature and 0.004 for salinity on the shelf, and 0.002°C and 0.002, respectively, in deeper water.

Water samples were taken for O_2 concentration using standard Winkler titrations for sensor calibration and for a suite of biogeochemical properties, including nutrients, dissolved inorganic carbon (DIC), chlorophyll *a* (Chl *a*), and particulate organic carbon (POC). Methods for these analyses are briefly presented below, with additional detail provided by Arrigo et al. (2014).

Currents were measured on both cruises using *Healy's* hull-mounted Ocean Surveyor 150 KHz acoustic Doppler current profiler (ADCP). The data were acquired using the UHDAS software package from the University of Hawaii, with additional processing done using the CODAS3 software utility (http://currents.soest.hawaii.edu). Following this, the barotropic tidal signal was removed from each profile using the Oregon State University model (http://volkov.oce.orst.edu/tides; Padman and Erofeeva, 2004). The uncertainty of the final product is estimated to be ±2 cm s^{-1}.

Nutrients and dissolved inorganic carbon. Discrete water column samples were analyzed for nutrients on board the ship with a Seal Analytical continuous-flow AutoAnalyzer 3 using a modification of the method of Armstrong et al. (1967). In this study, we focus primarily on nitrate (NO_3^-), but also consider concentrations of silicate ($Si(OH)_4$) and phosphate (PO_4^{3-}). Seawater samples for DIC were collected at each station into pre-cleaned ~300 mL borosilicate bottles, poisoned with $HgCl_2$ to halt biological activity, and then sealed after the cast. The analysis was done post-cruise at the Bermuda Institute of Ocean Sciences (BIOS) using a highly precise (~0.025%; <0.5 mmol kg^{-1}) gas extraction/coulometric detection system (Bates et al., 2005), along with Certified Reference Materials (provided by A. G. Dickson, Scripps Institution of Oceanography). The resulting accuracy was 0.05% (~0.5 mmol kg^{-1}).

Phytoplankton. Samples for Chl *a* were filtered onto 25 mm Whatman GF/F filters (nominal pore size 0.7 µm), placed in 5 mL of 90% acetone, and then extracted in the dark at 3ºC for 24 hrs. Chl *a* was measured fluorometrically (Holm-Hansen et al., 1965) on-board using a Turner 10-AU fluorometer (Turner Designs, Inc.) calibrated with pure Chl *a* (Sigma). POC samples

were collected by filtering water samples onto pre-combusted (450°C for 4 hrs) 25 mm Whatman GF/F filters. Filter blanks were produced by passing ~50 mL of 0.2 μm filtered seawater through a GF/F. All filters were then immediately dried at 60°C and stored dry until analysis. Prior to analysis, samples and blanks were fumed with concentrated HCl, dried at 60°C, and packed into tin capsules (Costech Analytical Technologies, Inc.) for elemental analysis on an Elementar Vario EL Cube (Elementar Analysensysteme GmbH, Hanau, Germany) interfaced to a PDZ Europa 20-20 isotope ratio mass spectrometer (Sercon Ltd., Cheshire, UK). Standards included peach leaves and glutamic acid.

At select stations, we also determined the maximum efficiency of photosystem II (Fv:Fm) from discrete water column samples by fast repetition rate fluorometry (FRRf) (Kolber et al., 1998), with excitation at 470 nm. These samples were collected, dark acclimated for ~30 min at *in situ* temperatures, and measured on the FRRf within one hour of collection. Blanks for individual samples analyzed by FRRf were prepared by gentle filtration through a 0.2 μm polycarbonate syringe filter before measurement using identical protocols. All Fv:Fm values were corrected for blank effects (Cullen and Davis, 2003).

2.3. Classification of winter water

Consistent with several companion studies (Pickart et al., submitted; Brown et al., this issue; Mills et al., this issue), WW is defined here as the water with potential temperature (θ) below -1.6°C. This distinguishes the most recently ventilated, and therefore most pure, WW from the modified (via solar heating and/or mixing with summer water masses) 'remnant' WW (-1.6°C < θ < -1°C) also found on the Chukchi shelf in the summer (Gong and Pickart, this issue). We note that related studies (e.g. Brown et al., this issue; Mills et al., this issue; Strong et al., submitted) exclude waters with relatively low NO_3^- (<10 μmol L^{-1}) from the definition of WW to avoid misidentifying cold, near-surface sea ice melt water. However, in the seven transects of this study, all near-surface (<10 m) water samples colder than -1.6°C were characterized by salinities greater than 31.5 and were part of a continuous water mass that extended from depth to the

surface. For this reason, we include all samples meeting the temperature requirement ($\theta \leq$ -1.6°C) in our definition of WW, regardless of nutrient content.

2.4. Hydrographic analysis

Vertical sections of water column variables were constructed using either the DIVA gridding package in Ocean Data View 4 (Schlitzer, 2014) or a Laplacian-spline interpolator (see Pickart et al., 2013). We consider sections of θ, salinity, absolute geostrophic velocity, NO_3^-, DIC, Chl *a*, POC, and O_2 saturation (calculated in Ocean Data View 4), focusing on the upper 60 m of the water column. The absolute geostrophic velocity was calculated by referencing the gridded thermal wind shear to the gridded cross-transect ADCP velocity for each grid pair across the section. To illustrate stratification and mixing processes and the location of WW in relation to our biogeochemical measurements, the hydrographic sections are overlain by contours of potential density (σ_θ; kg m^{-3}, thin lines) and the delimiting WW isotherm (θ=-1.6°C, thick line). For stations with bottom depths shallower than 60 m, the seafloor is indicated by a dark gray color on the hydrographic section plots and the vertical region between the deepest sample and the seafloor is illustrated in light grey. The statistical significance of differences between WW and non-WW samples for each transect were assessed through a series of T-tests following log transformation of the data.

2.5. Open water duration

Annual cycles of sea ice concentration for 2010 and 2011 were obtained at each station from daily AMSR-E (Advanced Microwave Scanning Radiometer – Earth Observing System) satellite images at 12.5 km resolution, accessed from the National Snow and Ice Data Center (NSIDC). The sea ice concentrations at each station were then used to calculate open water duration, defined as the number of days that the station location had <50% ice concentration between the date of initial ice retreat and the sampling date. In cases where ice retreated and re-advanced over a particular location before the final retreat (due to wind shifts, for example), we did not

include those periods with >50% concentration. Calculated in this way, open water duration is a proxy for the amount of time that phytoplankton at a given station were exposed to the full incident sunlight of the open water environment, as opposed to the lower light conditions present underneath sea ice. For a detailed justification of the 50% ice concentration threshold used to distinguish open water from ice cover in this region, see Lowry et al. (2014). Plots of open water duration are presented along with the hydrographic sections to provide environmental context for each transect.

3. Results

3.1. Presence and flow of WW

For the seven transects considered in this study, WW was found at 78% (82 of 105) of the stations, demonstrating the prevalence of this water mass laterally throughout our study region. However, WW was observed at only 35% (1678 of 4833) of the one-meter CTD bins in the upper 60 m, a consequence of the non-uniform vertical distribution of WW. WW was frequently observed at depth but was found much less commonly near the surface during our summer sampling period. The salinity range of the WW was relatively wide (31.23-33.38) and overlapped with the salinity range of nearby warmer water.

The flow pathways of WW across the Chukchi shelf observed during the ICESCAPE program were identified and mapped by Pickart et al. (submitted). The main pathways are included in Fig. 1. Much of the WW on the northeast shelf drains through Barrow Canyon (e.g. Pickart et al., 2005; Weingartner et al., 2005). However, as described by Pickart et al. (submitted), the precise flow paths leading to the canyon are more complex than previously thought. As seen in Fig. 1, a branch of WW enters our study area from the west, presumably emanating from the western-most branch (Pickart et al., 2010), and joins the Central Channel WW pathway. As this combined flow encounters Hanna Shoal it bifurcates, with a portion circulating cyclonically around the shoal and the rest being diverted southward. The southward

247 limb is then believed to turn eastward to join the coastal branch of WW before flowing into
248 Barrow Canyon en route to the Arctic Basin.
249
250 *3.2. Vertical sections*
251 Next, we relate the location and nature of the flow of WW through each transect to the
252 various physical and biogeochemical properties, using vertical sections of salinity, nutrients,
253 DIC, phytoplankton biomass, and O_2 saturation, as well as plots of satellite-derived open water
254 duration. We begin our description with the southernmost transect and then follow the pathway
255 of WW around the northern side of Hanna Shoal (Fig. 1).
256
257 *3.2.1. Central Channel*
258 The southernmost transect extended west to east across Central Channel to the vicinity of the
259 Alaskan coast (from left to right; Figs. 1, 2A, and 3). Potential temperature along the Central
260 Channel transect (Fig. 3A) revealed that WW was present at three distinct locations (the thick
261 black contour in the vertical sections marks the -1.6°C isotherm, which is the upper limit of
262 WW). The absolute geostrophic velocity (Fig. 2A) indicated that the largest volume of WW
263 (located to the west) was flowing to the north within the Central Channel pathway (Fig. 1) at
264 speeds as large as 15-20 cm s^{-1}. A smaller volume of WW was progressing southward at a
265 relatively slow speed ($\leq$5 cm s^{-1}), likely due to a small recirculation from the main pathway
266 (Figs. 1 and 2A; see also Pickart et al., submitted). The smallest pathway of WW (located to the
267 east) was also flowing northward, advected by the Alaskan Coastal Current at speeds ranging
268 from 15 to 20 cm s^{-1}.
269 The temperature of WW generally decreased with depth. The salinity range of WW in the
270 Central Channel transect was 32.40 - 33.25 (Fig. 3B). The highest salinity WW was located in
271 the Central Channel pathway, while fresher WW was advected by the Alaskan Coastal Current.
272 Note that a small amount of high salinity water (~33.30) was also found in warmer (~0°C)
273 bottom waters near the coast of Alaska (St. 55; Fig. 3B), indicating that WW was not always the

highest salinity water mass on the Chukchi shelf. The mean potential density of the WW (σ_θ = 26.46 ± 0.13 kg m^{-3}) was significantly higher ($p<0.001$) than that of the non-WW (σ_θ = 25.70 ± 0.63 kg m^{-3}), a pattern that was generally true of all seven transects (Table 1).

WW was rich in dissolved nutrients, with all three pathways containing higher concentrations of NO_3^- (Fig. 3C), silicate (not shown), and phosphate (not shown) than the adjacent warmer water. Nutrients were highest at the westernmost stations within the Central Channel WW pathway (Figs. 1 and 3C), with a maximum NO_3^- concentration of 14.7 µmol L^{-1}, and lowest at the easternmost stations within the Alaskan Coastal Current, with a maximum NO_3^- concentration of 11.9 µmol L^{-1}. The mean WW NO_3^- concentration for all of the stations along the transect (12.0 ± 1.71 µmol L^{-1}) was nearly 6.5-fold higher ($p<0.001$) than that of the non-WW (1.85 ± 3.15 µmol L^{-1}; Table 1). Notably, the Central Channel transect had the highest non-WW mean NO_3^- concentration of all seven transects (Table 1; $p<0.01$), due to the substantial presence of remnant WW (-1.6°C < θ < -1°C) that was elevated in NO_3^- (Fig. 3A and 3C). Concentrations of DIC (Fig. 3D) were also elevated along the WW pathways. On average, WW DIC concentrations in this transect were 155 µmol L^{-1} higher than that of non-WW, with a mean value of 2203 ± 52 µmol L^{-1} for WW and 2048 ± 101 µmol L^{-1} for non-WW (Table 1; $p<0.001$). The vertical sections of both NO_3^- and DIC show evidence of substantial biological uptake in the upper 20 m of the water column.

There were three distinct areas of elevated phytoplankton biomass in the Central Channel transect (Fig. 3E and 3F), each in close proximity to a respective WW pathway. The large phytoplankton bloom associated with the northward flowing Central Channel WW pathway (St. 38-43) had the highest biomass, with Chl *a* (Fig. 3E) and POC (Fig. 3F) concentrations of 16-30 µg L^{-1} and 70-100 µmol L^{-1}, respectively, that extended from the surface down to the interface between WW and non-WW at 13-20 m depth. Biomass was also elevated at the interface of the southward flowing WW pathway at 25 m depth (15.3 µg Chl *a* L^{-1} at St. 48) and immediately inshore of the WW in the Alaskan Coastal Current at 32 m depth (8.80 µg Chl *a* L^{-1} at St. 53). The lowest concentrations of phytoplankton (e.g. <1 µg Chl *a* L^{-1}; Fig. 3E) were found in surface

301 waters that were depleted in nutrients (e.g. upper 15-20 m; St. 44-55) and in the light-limited
302 WW (at 25-50 m depth) shaded by the large phytoplankton bloom in St. 38-43. WW in the
303 Central Channel transect had lower phytoplankton biomass than non-WW (Table 1), based on
304 POC concentrations of 18.7 ± 12.4 μmol L^{-1} and 36.3 ± 33.1 μmol L^{-1}, respectively (p=0.02).
305 Mean concentrations of Chl *a* for WW and non-WW were 3.53 ± 3.75 μg L^{-1} and 5.40 ± 8.53 μg
306 L^{-1}, respectively, although these values did not represent a statistically significant difference. We
307 note that the large phytoplankton bloom above the WW in the Central Channel pathway (St. 38-
308 43) greatly influenced the non-WW means of this transect.
309 The O_2 saturation (Fig. 3G) was highest (140-175%) within the large phytoplankton bloom
310 (St. 38-45). Despite the low biomass in the surface waters east of this bloom (St. 44-55), the
311 upper water column was supersaturated (>100%) with O_2, indicative of recent photosynthesis
312 throughout the transect. The observations of low POC and Chl *a* in the upper water column
313 paired with high O_2 saturation indicate that photosynthesis was likely followed by the sinking of
314 phytoplankton cells to deeper in the water column, resulting in the higher biomass within WW at
315 these stations. Across the Central Channel transect, the mean O_2 saturation was higher in non-
316 WW (114 ± 14.4%) than in WW (90.7 ± 6.8%) ($p<0.001$), revealing a pattern of supersaturation
317 in the non-WW and undersaturation in WW. This pattern was consistent for all of the transects
318 in this study (Table 1).
319 The satellite-derived open water duration (defined earlier in section 2.5) reveals that there
320 was large variation in the timing of ice retreat, with open water duration increasing markedly
321 from west to east across the Central Channel transect (Fig. 3H). Waters where the large upper
322 water column phytoplankton bloom was located (St. 38-43) were recently ice-covered (e.g. only
323 one day of open water at St. 38 where Chl *a* concentrations were 16-25 μg L^{-1}); by contrast,
324 waters with deeper and lower biomass (St. 44-55) had been open for much longer (e.g. 42 days at
325 St. 48 and 50 days at St. 53).
326
327 *3.2.2. Chukchi North*

328 Located north of the Central Channel transect, the Chukchi North transect extended
329 northwest to southeast across the Chukchi shelf (from left to right; Figs. 1, 2B, and 4) and was
330 characterized by WW in two distinct locations (Fig. 4A). The larger of the two WW pathways
331 was flowing poleward at speeds ranging from 10-20 cm s^{-1}. This is the northward extension of
332 the Central Channel pathway with a contribution from the western-most pathway that has been
333 diverted eastward from Herald Canyon, due to the topography of the shelf (Pickart et al., 2010;
334 Pickart et al., submitted; Fig. 1), The smaller WW pathway was progressing southward from the
335 northern Chukchi shelf at a slower speed ($\leq$5 cm s^{-1}) (Figs. 1, 2B, and 4A).
336 The salinity range of WW in this transect (31.63-33.25) was greater than that of the Central
337 Channel transect, due primarily to the lower salinity WW near the surface in the northwestern
338 stations (54-53) where WW was present throughout the entire water column (Fig. 4B). The
339 Chukchi North WW was colder than that of the previous transect ($p<0.001$), with a mean θ of -
340 1.72 ± 0.05°C (Table 1).
341 Concentrations of NO_3^- (Fig. 4C), silicate (not shown), phosphate (not shown), and DIC (Fig.
342 4D) were related to the distribution of WW, with the depth of the nutricline and the largest DIC
343 gradient mirroring the vertical extent of WW in each of the two pathways. NO_3^- concentrations
344 in this transect were seven-fold higher in WW than in non-WW ($p<0.001$), with mean values of
345 12.1 ± 6.27 µmol L^{-1} and 1.73 ± 3.76 µmol L^{-1}, respectively (Table 1). The northwestern stations
346 where WW extended to the surface (St. 54-53) displayed the greatest variation in WW nutrients
347 and DIC, with concentrations ranging from ~0 µmol NO_3^- L^{-1} and 2010 µmol DIC L^{-1} at the
348 surface to 19.7 µmol NO_3^- L^{-1} and 2270 µmol DIC L^{-1} at depth.
349 Concentrations of Chl *a* (Fig. 4E) and POC (Fig. 4F) showed two distinct phytoplankton
350 blooms associated with the two WW pathways, with bloom depth related to the vertical extent of
351 WW. For example, at stations where WW was present near the surface (St. 54-53; 43-42), the
352 Chl *a* and POC maxima were near the surface. As the WW isotherm deepened towards the
353 seafloor (e.g. St. 49-48; 40-38), the depth of maximum biomass also deepened. Note that the
354 apparent discrepancy between Chl *a* and POC data at St. 49 (at ~35 m depth) in Fig. 4 is an

355 artifact of the absence of POC data at that station. Unlike the Central Channel transect where the
356 highest biomass was located primarily above the WW, blooms along the Chukchi North transect
357 had high biomass (10-50 μg Chl *a* L^{-1}) both at the interface with and within the WW, resulting in
358 a mean Chl *a* concentration that was 3.4 times higher ($p<0.001$) in WW than in non-WW (7.98 ±
359 9.56 μg L^{-1} and 2.35 ± 3.50 μg L^{-1}, respectively; Table 1). Phytoplankton abundances were low
360 (<1 μg Chl *a* L^{-1} and <15 μmol POC L^{-1}) throughout the water column where WW was not
361 present (St. 47-44), in NO_3^--depleted non-WW above the subsurface blooms, and in the light-
362 limited WW beneath the near-surface bloom in the northwest (St. 54-52).
363 Similar to the previous transect, the upper water column was supersaturated in O_2, with
364 higher O_2 saturation (maximum: 144%) between the surface and the WW isotherm (Fig. 4G). O_2
365 was also supersaturated within WW near the sea surface (upper 15-20 m) at St. 54-53, in contrast
366 to the previous transect where all WW was undersaturated in O_2. Even at stations where
367 phytoplankton biomass was low and there was no WW, O_2 was supersaturated (102-125%; St.
368 46-48) and nutrients were depleted except near the seafloor, signaling previous photosynthesis
369 throughout the upper water column of all stations along the Chukchi North transect. Despite the
370 high biomass contained within WW, O_2 saturation was lower in WW than in non-WW
371 ($p<0.001$), with mean values of 95.3 ± 10.9% and 112 ± 11.7%, respectively (Table 1).
372 Ice retreat across the Chukchi North transect (Fig. 4H) was characterized by two regions
373 where open water duration increased from west to east: stations 54-44 (0-15 days) and stations
374 43-36 (5-31 days). Interestingly, both of these increases were correlated with the vertical extent
375 of water column biogeochemical properties (Fig. 4A-G). In particular, the depth of maximum
376 phytoplankton biomass, the WW isotherm, and the nitracline were shallowest at stations that
377 were either still ice-covered or recently ice-free, and deepest at stations with longer open water
378 duration. We note that the northwestern bloom (St. 54-48) comprised a portion of the massive
379 under-ice phytoplankton bloom that extended 100 km farther into the fully consolidated ice pack,
380 as described by Arrigo et al. (2012; 2014). The fact that the southeastern bloom (St. 43-36)

displayed a similar relationship between biogeochemical properties and open water duration suggests that this bloom likely also initiated underneath the ice (see Section 4.3 below).

3.2.3. Chukchi Slope West

The longest and most northern transect extended northwest to southeast from the upper continental slope (~150 m depth) across the Chukchi shelfbreak to the shallow water (~40 m) northwest of Hanna Shoal (from left to right; Figs. 1, 2C and 5). WW was flowing weakly to the west (<10 cm s^{-1}; Fig. 2C) at the northern end of the transect due to wind-driven upwelling that reversed the (normally eastward-flowing) shelfbreak jet (Spall et al., 2014). At the time of occupation of the section, the eastward flow of the jet was starting to become re-established at deeper levels in the water column. On the shelf, the circulation of WW was the same as observed on the Chukchi North section; i.e., northeastward flowing WW adjacent to equatorward-flowing WW closer to Hanna Shoal (compare Figs. 2B and 2C shoreward of the shelfbreak). Although restricted to the bottom 10 m at St. 70-72, WW was present at all stations along this ~300 km long transect (Fig. 5A).

The Chukchi Slope West transect exhibited the widest range in WW salinity, NO_3^-, and DIC (Fig. 5B-D). Similar to previous transects, WW NO_3^- concentrations were high (mean: 12.7 ± 6.21 μmol L^{-1}; Table 1) and the nitracline and the DIC gradient approximately mirrored the WW isotherm (Fig. 5C and 5D). The highest maximum NO_3^- concentrations on the shelf (upper 60 m) were measured in this transect, with a maximum value of 20.2 μmol L^{-1} in WW at St. 66. Surface waters were depleted in NO_3^- (~0 μmol L^{-1}), even where WW extended to the surface (St. 60-61).

A massive phytoplankton bloom was evident along the Chukchi Slope West transect, with Chl *a* and POC values of 15-30 μg L^{-1} and 50-100 μmol L^{-1}, respectively, throughout most of the upper 30-40 m of the water column (Fig. 5E and 5F). Biomass was lowest (<0.5 μg Chl *a* L^{-1}) at stations where WW was at its minimum vertical extent (St. 68-72). Despite low light conditions caused by shading from the bloom above, concentrations of Chl *a* were relatively high in WW on

408 the shelf beneath the massive phytoplankton bloom (St. 59-68; e.g. 40-60 m), with minimum Chl
409 *a* concentrations of 1-2 μg L^{-1} and some as high as 5-10 μg L^{-1}. As with the previous transect,
410 phytoplankton biomass was concentrated near the interface between WW and non-WW (Fig. 5E
411 and 5F).
412 O_2 saturation was very high throughout the upper water column (Fig. 5G) in both WW and
413 non-WW, with values as high as 130-150% between the surface and 25-30 m in the northwestern
414 portion of the transect. At stations where the WW isotherm was deepest, O_2 saturation was
415 highest 10-20 m above the WW (St. 70-72). Similar to previous transects, O_2 was undersaturated
416 in bottom WW. However, due to the high levels of O_2 produced in WW by the massive
417 phytoplankton bloom at St. 57-69, this transect yielded the highest mean WW O_2 saturation of all
418 seven transects ($p<0.05$), with a mean of 97.9 ± 17.0% (Table 1). Similarly, the O_2 saturation in
419 non-WW was also very high, with a mean of 117 ± 11.6%.
420 The northwestern half of the Chukchi Slope West transect was still ice-covered at the time of
421 sampling (Fig. 5H), with zero days of open water duration at St. 57-65 where the massive under-
422 ice phytoplankton bloom was observed (Arrigo et al., 2012; 2014). Similar to the previous
423 transect, there was a clear relationship between open water duration, the depth of the bloom, and
424 the vertical extent of WW: both WW and the bloom reached the surface underneath the ice (St.
425 60-61) and extended deeper at stations with longer open water duration (e.g., St. 68-70, with 6-9
426 days open water duration, a WW isotherm depth of 25-39 m, and a biomass maximum of 35-45
427 m).
428 At three stations along the Chukchi Slope West transect, we also measured vertical profiles
429 of the maximum efficiency of photosystem II (Fv:Fm) of phytoplankton (Fig. 6). Fv:Fm values
430 were highest either at or slightly below the interface between WW and non-WW, where NO_3^-
431 concentrations were high and light availability was sufficient for photosynthesis. In contrast,
432 Fv:Fm values were lowest in the upper water column where light levels were high but nutrients
433 were depleted (~0 μmol NO_3^- L^{-1}), and in deeper waters where NO_3^- availability was high but
434 light was limiting. For example, at St. 62 where WW was present in the upper water column,

435 Fv/Fm was highest (0.53) several meters below the WW isotherm, reflecting the fact that
436 phytoplankton growth had already depleted nutrients from shallower WW prior to our sampling.
437
438 *3.2.4. Hanna Shoal North*
439 Located east of the Chukchi Slope West transect, the Hanna Shoal North section extended
440 northwest to southeast from just beyond the shelf edge toward Hanna Shoal (from left to right;
441 Figs. 1, 2D, and 7A). WW was observed at all stations. During our sampling period, the
442 shelfbreak jet was fully re-established and advecting WW to east fairly rapidly (>20 cm s^{-1}).
443 Because of the relatively short distance between Hanna Shoal and the shelf edge, the eastward
444 flowing pathway of WW on the outer shelf was not a distinct feature (as it was in the previous
445 two transects), but instead was located immediately adjacent to the shelfbreak jet (Fig. 2D).
446 Inshore of this, the WW returned southward next to Hanna Shoal as it had in the Chukchi Slope
447 West section.
448 Phytoplankton biomass was high throughout the WW in this transect (Fig. 7E), with a mean
449 Chl *a* concentration of 10.4 ± 6.02 μg L^{-1} (Table 1). By contrast, biomass was relatively low in
450 the upper 20 m of the water column, with a mean non-WW Chl *a* concentration of 1.66 ± 1.36
451 μg L^{-1} (more than 6-fold lower than that of WW; $p<0.001$). We note that the apparent
452 discrepancy between POC and Chl *a* concentrations results from a lack of POC data at St. 77 and
453 St. 79 (Fig. 7E and 7F). Similar to previous transects, phytoplankton biomass was concentrated
454 at the interface between WW and non-WW, with the highest Chl *a* concentrations just below the
455 WW isotherm (Fig. 7E).
456 O_2 was supersaturated throughout the upper water column, with high O_2 saturation extending
457 from the surface to just below the WW isotherm (Fig. 7G). As with the previous transect, O_2
458 saturation generally increased with depth towards the WW, with the highest values found just
459 above the WW isotherm. Within WW, O_2 saturation decreased with depth towards the seafloor.
460 This transect exhibited the highest non-WW mean O_2 saturation (119 ± 8.9%; Table 1) of the

study ($p<0.05$), signaling previous photosynthesis by phytoplankton despite the low biomass in non-WW relative to WW.

Most stations along this transect were sampled relatively soon after ice retreat (Fig. 7H). Only the southernmost station closest to Hanna Shoal had been open for more than a week prior to sampling (11 days; St. 82). This station also had the least amount of WW. Conversely, the northernmost stations (St. 76-77) were still ice covered at the time of sampling and had the greatest amount of WW. Between these two end points, the remaining stations (St. 78-81) had been open for 2-6 days prior to sampling and had a moderate amount of WW remaining on the shelf.

3.2.5. Chukchi Slope Center

Extending northeast to southwest from the base of the continental slope (~2000 m) to the shallow waters (~35 m) of Hanna Shoal, the Chukchi Slope Center transect was located east of the Hanna Shoal North transect (Fig. 1). WW was observed in the eastward-flowing shelfbreak jet, but not seaward of this. On the shelf, WW was once again being advected eastward in a distinct pathway, but the return flow was absent at this location since the transect was situated to the east of the bifurcation point of WW associated with Hanna Shoal (Fig. 1). As described by Pickart et al. (submitted), the WW advected in the shelf pathway at the Chukchi Slope Center section was noticeably fresher than farther to the west (i.e. upstream), resulting in a lower mean WW salinity in this transect (32.39 ± 0.21) than in the previous transects (Table 1). Additionally, non-WW in this transect was the freshest and least dense of all seven transects (Table 1), with a mean salinity of 29.77 ± 1.47 and a mean σ_θ of 23.93 ± 1.19 kg m^{-3} due in large part to the fresh and buoyant water sampled in the upper 20 m off the shelf in the northeastern stations.

The maximum concentrations of NO_3^- and DIC were associated with WW (Fig. 8C and 8D), although slightly elevated concentrations of NO_3^- (~1 μmol L^{-1}) and DIC (~2150 μmol L^{-1}) were also found in non-WW at 40-60 m depth along the shelfbreak (St. 99-93) due to the upward tilt

of the isopycnals progressing onshore. This transect contained very high concentrations of WW NO_3^- and DIC relative to the other transects, with means of 13.7 ± 3.61 μmol L^{-1} and 2252 ± 16 μmol L^{-1}, respectively (Table 1). The difference between mean NO_3^- in WW and non-WW (0.51 ± 1.50 μmol L^{-1}) was more than 25-fold ($p<0.001$), illustrating the extreme nutrient content of WW in relation to warmer waters on the Chukchi shelf.

Extremely high WW mean values of Chl *a* (14.2 ± 19.8 μg L^{-1}) and POC (44.9 ± 55.1 μmol L^{-1}) were observed on the Chukchi Slope Center transect (Table 1). These mean values were greatly influenced by an extremely large phytoplankton bloom at the interface between WW and non-WW (St. 85-83), with maximum concentrations of Chl *a* (77.0 μg L^{-1} at St. 83) and POC (155 μmol L^{-1} at St. 84) that were the highest of the study (Fig 8E and 8F). Conversely, biomass was very low in non-WW (except for 10-20 m above the WW isotherm), yielding non-WW mean values that were the lowest of the study (0.61 ± 1.58 μg Chl *a* L^{-1} and 5.7 ± 7.3 μmol POC L^{-1}; $p<0.01$). The difference between Chl *a* concentrations in WW and non-WW was 23-fold ($p<0.001$), resembling the difference in NO_3^- concentrations described above.

Open water duration was extremely short in this transect, with the majority of stations still under ice cover at the time of sampling (zero days of open water duration at St. 99-86). The southwestern stations near Hanna Shoal (St. 85-83), where the massive phytoplankton bloom was located, were sampled in open water within 3-6 days of sea ice retreat. There were only 5-6 days of open water prior to sampling at St. 84-83, where the maximum phytoplankton biomass was the highest of this study (73-77 μg Chl *a* L^{-1}).

3.2.6. Chukchi Slope East

Spanning the northeastern portion of the Chukchi Sea, the Chukchi Slope East transect extended northeast to southwest from the upper slope (~350 m) to the shallow waters (~25 m) of Hanna Shoal (from left to right; Figs. 1, 2F, and 9). A single region of WW was located in the center of this transect within the bottom 15-20 m of the water column. The seaward portion of the WW was being advected by the shelfbreak jet, while the shoreward portion was contained in

515 the shelf pathway advecting the cold water cyclonically around Hanna Shoal (Figs. 1 and 2F).
516 The mean θ (-1.70 ± 0.04 °C) and salinity (32.41 ± 0.21) of WW in the Chukchi Slope East
517 transect was almost identical to that of the Chukchi Slope Center transect (Table 1), indicating
518 that there was little modification of the WW as it progressed between the two transects. The
519 range of non-WW salinity (19.74-32.49) was the largest here of all seven transects, with the
520 freshest values at the surface near the shelfbreak (St. 106-108; Fig. 9B), indicating recent sea ice
521 melt.
522 Consistent with previous transects, NO_3^- and DIC concentrations were extremely high within
523 WW (Table 1), although relatively high concentrations were also found in the northeastern
524 stations on the shelfbreak (St. 102-105) where WW was not present (Figs. 9C and 9D).
525 Nutrients and DIC were depleted in non-WW in the upper 20-30 m of the water column (~0
526 μmol $NO_3^- L^{-1}$ and 1950 μmol DIC L^{-1}). The maximum NO_3^- concentration in this transect was
527 18.5 μmol L^{-1}, the same as the maximum WW concentration along the Chukchi Slope Center
528 transect.
529 There was a subsurface phytoplankton bloom associated with the nutrient-rich WW,
530 illustrated by high concentrations of Chl *a* and POC (Fig. 9E and 9F). Biomass was most
531 concentrated at the WW isotherm, with a maximum of 30.6 μg Chl *a* L^{-1} at St. 110 where WW
532 was at its shallowest extent (27 m depth). Biomass was relatively low at St. 106-107, where
533 WW was confined to the light-limited waters below 40 m, and at St. 102-105 on the shelfbreak,
534 where WW was not present. Mean Chl *a* and POC concentrations in WW were very high (10.8
535 ± 9.51 μg L^{-1} and 39.4 ± 29.8 μmol L^{-1}, respectively; Table 1).
536 Stations at or near the shelfbreak were still ice-covered during our sampling period, with zero
537 days of open water at St. 102-107. The remaining stations (St. 108-115) had been ice-free for 4-
538 17 days, with open water duration increasing from northeast to southwest. The station with the
539 highest biomass (>30 μg Chl *a* L^{-1}) and the largest extent of WW had been open for 12 days
540 prior to sampling (St. 110), while stations closest to Hanna Shoal with no WW remaining on the
541 shelf had been open for longer (15-17 days).

542

543 *3.2.7. Hanna Shoal Southeast*

544 The final section sampled along the anti-cyclonic WW pathway around Hanna Shoal was the
545 Hanna Shoal Southeast transect, which extended southwest to northeast from the vicinity of
546 Barrow Canyon towards Hanna Shoal (from left to right; Figs. 1, 2G, and 10). Although the
547 outer shelf advection pathway was quite evident in this transect (Fig. 2G), only a small amount
548 of WW was present within the pathway at the time of our sampling. This implies that the Hanna
549 Shoal Southeast transect was near the leading edge of the WW at this point in the summer
550 season, such that there was no WW downstream of this transect during our sampling period (as
551 described in more detail in Pickart et al. (submitted)). While the mean salinity of WW was
552 similar to that of the previous two transects (Table 1), the mean potential temperature (-1.64 ±
553 0.03°C) was the highest of all seven transects ($p<0.001$) and the density was the lowest (σ_θ:
554 25.98 ± 0.15 kg m^{-3}) ($p<0.001$). This transect contained only a small amount of WW rich in
555 NO_3^- (Fig. 10C), with a relatively low mean of 9.78 ± 4.45 μmol L^{-1} (Table 1). Although still
556 high, the maximum NO_3^- value (13.8 μmol L^{-1}) was also the lowest maximum of all seven
557 transects. In contrast, although DIC concentrations followed a similar pattern to NO_3^-, the mean
558 WW DIC concentrations were not the lowest on the shelf (Table 1).

559 Phytoplankton abundance (Fig. 10E and 10F) was elevated at stations where WW was
560 present and within remnant WW near the seafloor. There were two locations with very high
561 phytoplankton biomass (St. 120 at 16 m and St. 124 at 40 m; both ~30 μg Chl *a* L^{-1}). The bloom
562 at St. 120 was concentrated at ~18 m depth, where a small amount of WW provided a source of
563 NO_3^- in an otherwise nutrient-depleted section of the upper water column. The bloom at St. 124
564 was located at the northwestern boundary of the WW, although the highest biomass was
565 contained in remnant WW at the time of sampling.

566 Consistent with the previous six transects, O_2 saturation increased near the WW isotherm
567 (Fig. 10G). However, the mean values of O_2 saturation in both WW (85.6 ± 8.2) and non-WW

568 (105 ± 7.9) were very low (Table 1), with the latter value representing the lowest non-WW mean
569 of this study ($p<0.01$).
570 Every station in this transect had been ice-free for at least two weeks (Fig. 10H), with open
571 water duration increasing from 17 days at St. 115 (near Hanna Shoal) to 33 days at St. 125
572 (closest to the Alaskan coast). The relatively long open water duration of this transect, paired
573 with the relatively small amount of WW, depleted nutrients, and biomass mostly concentrated
574 near the seafloor, indicated that we sampled this location after substantial primary production
575 had already taken place. The only locations where phytoplankton continued to bloom were those
576 that were influenced by a supply of nutrient-rich WW.
577
578 **4. Discussion**
579 *4.1. Significance of nutrient-rich WW for phytoplankton blooms*
580 The overarching theme that emerged in this study was that the presence of extremely cold
581 WW ($\theta \leq -1.6$°C) was consistently associated with phytoplankton blooms. The relationship
582 between phytoplankton and WW was driven not by temperature but by the extremely high
583 nutrient content of this near-freezing water mass, particularly in the case of NO_3^-, which is the
584 primary limiting nutrient in the Chukchi Sea (Cota et al., 1996; Codispoti et al., 2005; Tremblay
585 et al., 2006). Plots of θ versus NO_3^- for all water samples in the seven transects described above
586 (Fig. 11A-G) illustrate that the highest concentrations of NO_3^- were found at extremely cold
587 temperatures. Although slightly warmer remnant WW (-1.6°C $< \theta < 0$°C) occasionally
588 contained relatively high nutrient concentrations, the vast majority of NO_3^- found on the Chukchi
589 shelf was associated with WW ($\theta \leq -1.6$°C), with most concentrations between 5-20 μmol L^{-1}.
590 Summer water masses ($\theta > 0$°C) contained virtually no NO_3^-, with concentrations frequently near
591 0 μmol L^{-1} and always <3.5 μmol L^{-1}. Across all seven transects, the mean NO_3^- concentration
592 was more than 10-fold higher in WW than in warmer water ($p<0.001$), with a mean of 12.3 ±
593 5.13 μmol L^{-1} (n=147) for WW and 1.13 ± 2.71 (n=306) for non-WW (Table 1). This
594 relationship was consistent between years, as demonstrated by the two transects that were

595 sampled in both 2011 and 2010: Chukchi North (Fig. 11B and 11H, respectively) and Hanna
596 Shoal North (Fig. 11D and 11I, respectively). Concentrations of other dissolved nutrients were
597 also very high in WW, although the relationship between water temperature and nutrient content
598 was most consistent in the case of NO_3^-. The mean silicate concentration in WW (37.3 ± 12.6
599 μmol L^{-1}) was nearly five times higher than that of non-WW (7.53 ± 7.89 μmol L^{-1}) ($p<0.001$).
600 Similarly, the mean phosphate concentration in WW (1.76 ± 0.39 μmol L^{-1}) was 2.4-fold greater
601 than that of non-WW (0.73 ± 0.31 μmol L^{-1}) ($p<0.001$). Thus, as WW flows across the Chukchi
602 shelf, it provides essential nutrients for phytoplankton that sustain primary production.
603 Driven by the high nutrient content of WW on the shelf, more phytoplankton biomass
604 accumulated in this water mass than in warmer, nutrient-poor water (Table 1). Across all seven
605 transects, the mean Chl *a* concentration was three-fold higher in WW (8.64 ± 9.75 μg L^{-1};
606 n=133) than in non-WW (2.79 ± 5.58 μg L^{-1}; n=285) ($p<0.001$). Concentrations of POC were
607 ~25% higher ($p<0.001$) in WW than in non-WW, with a mean of 25.0 ± 22.5 μmol L^{-1} (n=76)
608 and 19.2 ± 21.4 μmol L^{-1} (n=164), respectively. Similarly, although data are not shown for
609 individual transects, the mean concentration of particulate organic nitrogen (PON) was ~40%
610 higher in WW (4.00 ± 4.12 μmol L^{-1}; n=75) than in non-WW (2.67 ± 2.71 μmol L^{-1}; n=162)
611 ($p<0.001$). Phytoplankton physiology was also enhanced in nutrient-rich WW, with the mean
612 maximum efficiency of photosystem II (Fv:Fm) ~24% greater for phytoplankton sampled in
613 WW (0.494 ± 0.066; n=6) than for those in non-WW (0.389 ± 0.080; n=22) ($p=0.012$).
614 A second theme that emerged was that the vertical position of phytoplankton blooms in the
615 water column was dictated by the vertical extent of WW, with maximum phytoplankton biomass
616 concentrated at the interface between WW and non-WW (either at the same depth as or just
617 above/below the WW isotherm, illustrated in Figs. 3-5 and 7-10). This pattern demonstrates the
618 need of phytoplankton cells to balance nutrient availability with sufficient light for
619 photosynthesis. Although NO_3^- concentrations were more than 10-fold higher in WW than
620 adjacent non-WW, light availability was nearly 20-fold lower, with a mean PAR of 5.99 ± 44.9
621 μEin m^{-2} s^{-1} in WW (n=1678 one-meter light profile bins) compared to 114 ± 276 μEin m^{-2} s^{-1}

622 for non-WW (n=3155) ($p<0.001$). Consequently, the interface between deeper, nutrient-rich
623 WW and shallower, nutrient-poor water provided an balance between the competing needs of
624 phytoplankton in the Chukchi Sea for NO_3^- and sunlight, leading to the presence of surface
625 blooms at stations where WW was present in the upper water column and subsurface blooms at
626 stations where the interface between WW and non-WW was deeper. These results are consistent
627 with previous work demonstrating maximum phytoplankton biomass at the nitracline in the
628 Arctic (Tremblay et al., 2008; Martin et al., 2010; Ardyna et al., 2013), which, not surprisingly,
629 was mostly at the same depth as the interface between WW and non-WW in our study. For a
630 more detailed description of subsurface Chl *a* maxima (SCM) in the context of euphotic depth,
631 the nitracline, and mixed layer depth in the Chukchi and Beaufort Seas, see Brown et al. (this
632 issue).
633 A third theme consistent across the seven transects in this study was that the upper water
634 column was characterized by extremely high O_2 content, with O_2 saturation increasing towards
635 the interface between WW and non-WW and decreasing within the WW interior (resulting in the
636 characteristic supersaturation in non-WW and undersaturation in WW; Table 1). This feature
637 illustrates that, prior to our sampling, photosynthesis took place primarily in the upper water
638 column where light levels were optimal. By the time of our cruise, the supply of WW was
639 largely confined to the lower part of the water column. Consequently, the deepened WW
640 isotherm resulted in increased photosynthesis at greater depths and a sinking of phytoplankton
641 cells from shallower depths where nutrients were depleted. This pattern resulted in frequent
642 observations of extremely high phytoplankton biomass (e.g. 30 μg Chl *a* L^{-1}) within WW, with
643 very high O_2 saturation (e.g. 140%) near the interface between WW and non-WW where cells
644 were actively growing, and low O_2 saturation (e.g. 80%) in deeper waters, where biomass likely
645 accumulated primarily due to sinking processes. In these relatively deep waters, photosynthesis
646 was limited by reduced light availability from self-shading by the bloom above and thus, O_2
647 production by phytoplankton was not sufficient to balance O_2 losses through respiration.

Finally, to assess whether the relationship between WW and phytoplankton blooms was widespread in this region, we compared Chl *a* concentrations to measurements of potential temperature at all stations and depths sampled during the ICESCAPE program in 2010 and 2011 (Fig. 12). This approach added an additional 198 stations to the seven transects presented here and extended the geographic range to include samples from the southern Chukchi Sea, Barrow Canyon, and the western Beaufort Sea (for locations of all ICESCAPE stations, see Arrigo et al. (this issue)). Phytoplankton biomass was significantly higher at stations containing WW (at any depth in the water column) than at stations where WW was not present (Fig. 12), with depth-integrated Chl *a* concentrations that were 2.5-fold greater at WW stations (324 ± 294 mg m^{-2}; n=100) than at non-WW stations (133 ± 205 mg m^{-2}; n=202) ($p<0.001$). Similarly, mean Chl *a* concentrations throughout the water column were 2.8-fold greater at stations containing WW (Fig. 12; $p<0.001$). Thus, the presence of nutrient-rich WW was associated with higher phytoplankton biomass throughout the region across multiple years.

4.2. Contribution of WW to biological hotspots

In this study, we sampled WW that was transported across the Chukchi shelf via a number of different pathways, including those that traveled through the Central Channel, from Herald Canyon, and along the Alaskan Coastal Current. These three main WW pathways branched out within the Chukchi Sea into smaller filaments, producing the complex pathway of WW flow illustrated in Fig. 1 and described in detail in Pickart et al. (submitted). Many of these WW pathways ultimately converge in the northeastern Chukchi Sea, within the vicinity of the head of Barrow Canyon (Fig. 1). In fact, Barrow Canyon appears to be the primary outflow into the Arctic basin for WW that flows across the Chukchi shelf (Pickart et al., 2005; Weingartner et al., 2005; Gong and Pickart, submitted). Notably, the region of WW confluence in the northeastern Chukchi Sea is characterized by extremely high rates of benthic production that support an abundance of benthic-feeding seabird and marine mammal populations (Dunton et al., 2005;

674 Loeng et al., 2005; Grebmeier et al., 2006), leading to the classification of this region as a
675 macroinfaunal biomass 'hotspot' in the Pacific Arctic (Grebmeier et al., 2006, in prep.).
676 We suggest that the exceptional productivity of the northeastern Chukchi Sea is driven in
677 large part by the flow and confluence of multiple WW pathways in this region. Our study
678 illustrates that nutrient-rich WW fuels primary production across the Chukchi shelf, resulting in
679 phytoplankton blooms at all locations where WW intersected one of our seven transects. These
680 findings indicate that photosynthesis occurs continuously along WW flow pathways on the shelf,
681 leading to the accumulation of extremely high phytoplankton biomass within WW. Considering
682 that water column grazing rates are relatively low in the Chukchi Sea (Campbell et al., 2009;
683 Sherr et al., 2009), the high concentrations of phytoplankton contained in WW eventually sink to
684 the seafloor. Consequently, the convergence of multiple highly productive WW pathways in the
685 northeastern Chukchi Sea delivers a concentrated food source of sinking phytoplankton to the
686 benthic community over an extended period of time. Thus, the flow of phytoplankton-abundant
687 WW to the northeastern Chukchi Sea may play an essential and previously unrecognized role in
688 sustaining the richness of this biological hotspot.
689
690 *4.3. Evidence for under-ice blooms*
691 The massive phytoplankton bloom that we sampled underneath the ice in the northwestern
692 portion of the Chukchi Slope West and Chukchi North transects (Figs. 4 and 5) was the first fully
693 characterized under-ice bloom to be documented in the Chukchi Sea, as described previously
694 (Arrigo et al., 2012; 2014). In the seven transects presented here, there was additional evidence
695 of under-ice phytoplankton blooms at many stations that were either still ice covered or very
696 recently ice-free at the time of sampling. For example, the Chukchi North transect contained an
697 additional phytoplankton bloom with very high biomass (St. 43-37) located to the southeast of
698 the previously documented massive under-ice bloom (St. 54-49; Fig. 4). The magnitude and
699 vertical position of this phytoplankton bloom in relation to estimates of satellite-derived open
700 water duration indicate similar mechanisms of bloom formation and progression as the nearby

under-ice bloom. Thus, although sea ice had already retreated from the location of the southeastern bloom by the time we arrived, it is highly likely that this bloom also began beneath the ice, resulting in the measurements of elevated phytoplankton biomass at the surface in recently-ice free waters during our sampling period.

Comparing the magnitude of phytoplankton biomass in relation to open water duration at many additional stations also reveals evidence of under-ice blooms throughout the Chukchi Sea. For example, as described in Section 3.2.1, the large upper water column phytoplankton bloom in the Central Channel transect (Fig. 3) had very high biomass (16-25 μg Chl *a* L^{-1} and 70-85 μmol POC L^{-1}) at St. 38, which we sampled on the day after sea ice retreat. Similarly, phytoplankton biomass was very high (15-23 μg Chl *a* L^{-1}) at the interface between WW and non-WW in St. 76-79 in the Hanna Shoal North transect (Fig. 7), where open water duration was 0-3 days. In the Chukchi Slope Center transect (Fig. 8), Chl *a* concentrations exceeded 70 μg L^{-1} at St. 83 and 84, which had only been ice-free for 5-6 days. Across all seven transects comprising 105 stations, there were 21 stations with biomass >20 μg L^{-1}, with at least one station per transect. Open water duration at these stations was relatively short, with a mean of 9.14 ± 9.37 days. Such high biomass in recently ice-free waters implies that phytoplankton at many of these stations must have begun to grow underneath the ice, considering that an initial Chl *a* concentration of 0.02 μg L^{-1} at a relatively fast specific growth rate corresponding to a doubling per day (0.69 d^{-1}) would require two weeks to reach >20 μg Chl *a* L^{-1}.

Finally, O_2 saturation and nutrient concentrations indicate that phytoplankton bloomed in all shelf waters across the seven transects prior to our sampling, regardless of open water duration. O_2 was supersaturated throughout the upper water column, suggesting that widespread photosynthesis took place, even at stations that were still ice-covered or very recently ice free (e.g. in the Hanna Shoal North and Chukchi Slope Center transects). Similarly, NO_3^- and DIC concentrations were depleted throughout the upper water column, providing biogeochemical evidence of uptake by phytoplankton since the start of the growing season. Since open water duration was relatively short at many locations we sampled, these consistent signals of previous

728 phytoplankton growth provide additional evidence that there were under-ice blooms throughout
729 the study area prior to our sampling. The notion that under-ice blooms are prevalent in this
730 region is consistent with the satellite-based estimate that >70% of shelf waters in the Chukchi
731 Sea support phytoplankton blooms underneath sea ice prior to ice retreat (Lowry et al., 2014).
732
733 *4.4. Conceptual model of phytoplankton blooms in the Chukchi Sea*
734 The relationships between nutrient-rich WW, phytoplankton abundance, and open water
735 duration identified in this study, combined with previous work, allows for the construction of a
736 revised conceptual model of phytoplankton blooms in the Chukchi Sea.
737 In the winter, sea ice formation and brine rejection lead to convective overturning of the
738 shallow water column on both the Chukchi and Bering Sea shelves (Muench et al., 1988;
739 Weingartner et al., 1998; Woodgate et al., 2005b). This forms near-freezing WW and
740 replenishes the surface ocean with high concentrations of nutrients that are mixed into the water
741 column from the sediments. As the winter progresses, WW is advected into the Chukchi Sea
742 through Bering Strait, and polynyas and smaller leads open up locally on the Chukchi shelf
743 (Cavalieri and Martin, 1994; Iwamoto et al., 2014), which results in continued formation of WW.
744 Hence, by the end of the winter, presumably the water column is fully mixed with nutrient-rich
745 WW extending from the surface to the seafloor throughout much of the Chukchi shelf.
746 As sunlight returns to the ice-covered Chukchi Sea in the spring, solar heating begins to
747 modify sea ice and the underlying water column. Melt ponds form on the surface of the ice
748 (Polashenski et al., 2012, this issue), allowing sunlight to penetrate through the ice and into the
749 water column. As warming continues, melt ponds expand on the relatively flat first-year sea ice
750 that has become characteristic of the Chukchi Sea (Maslanik et al., 2011), increasing the
751 availability of sunlight in the upper ocean. Previous work reveals that up to 55% of incident
752 light is transmitted through first-year melt ponded ice (Frey et al., 2011). WW under the ice
753 warms slightly from its extremely cold formation temperature near -1.9°C, and also by mixing

754 with more moderate waters entering through Bering Strait (Gong and Pickart, 2012). In our
755 study, which took place in June/July, the mean observed WW temperature was -1.71 ± 0.05°C.
756 Once light availability under melt ponded ice is sufficient for primary production,
757 phytoplankton blooms begin in surface waters beneath the ice on the Chukchi shelf (Arrigo et al.,
758 2012; 2014, Palmer et al., 2014), fueled initially by the widespread presence of WW and
759 subsequently by the continued input of WW from the Bering Sea. As phytoplankton blooms
760 develop, O_2 is produced through photosynthesis and nutrients and DIC are utilized for
761 photosynthesis and cell growth. After NO_3^- is removed from surface waters, phytoplankton cells
762 cease growing and begin to sink, while new cells grow deeper in the water column where
763 nutrients are more abundant. This process continues as the blooms evolve, resulting in the
764 vertical 'migration' of blooms from the surface to the depth of the nitracline (Brown et al., this
765 issue). Although much of the phytoplankton biomass observed in this study was located in open
766 water and below the surface layer, the numerous observations of high O_2 saturation and depleted
767 $NO_3^-$and DIC concentrations throughout the upper water column (including at ice-covered
768 stations) indicate that blooms initiate earlier in surface waters throughout the Chukchi shelf,
769 likely under sea ice and within nutrient-rich water.
770 As spring transitions to summer and sea ice begins to retreat from the Chukchi Sea, WW is
771 increasingly modified through a combination of solar heating, mixing with summer water
772 masses, and nutrient uptake by phytoplankton. At the same time, WW is flushed off the Chukchi
773 shelf into the Canada Basin and replaced by summer water, so by mid-summer most of the WW
774 is confined primarily to the advective pathways illustrated in Fig. 1. The residence time of
775 nutrient-rich WW on the shelf depends largely on the flow speeds and length of the circulation
776 pathways; as such, phytoplankton bloom duration is determined in large part by circulation in the
777 Chukchi Sea. For example, based on hydrographic data collected in Barrow Canyon (Itoh et al.,
778 2015), cold Pacific-origin water travels quickly along the coastal pathway in the Chukchi Sea via
779 the Alaskan Coastal Current, which is consistent with previous studies (e.g. Weingartner et al.,
780 1998). In contrast, the cold water drains for a longer period (hence more slowly) through the

781 summer from the Central Channel pathway around the northern side of Hanna Shoal described
782 here (Fig. 1). Pickart et al. (submitted) compute an average advective speed of approximately 12
783 cm s^{-1} along this pathway, implying a travel time of over three months for the water to progress
784 from Bering Strait to the Hanna Shoal Southeast transect. Hence, this may explain the extended
785 duration of open water phytoplankton blooms in the Chukchi Sea, which were the longest of any
786 Arctic region from 1998-2009, with a mean of 119 ± 16.1 days (Arrigo and Van Dijken, 2011).
787 Like its residence time, the vertical extent of WW varies spatially in the summer, extending
788 to the surface at some locations and confined to deeper in the water column at others (with the
789 interface between WW and non-WW approximating the depth of the nitracline). The presence
790 and vertical position of phytoplankton were closely associated with the interface between WW
791 and non-WW, where the nitracline provides a balance between nutrients and light. Conversely,
792 the absence of WW on the shelf is accompanied by NO_3^- depletion, resulting in low
793 phytoplankton biomass. Presumably, after WW completely flushes off of the Chukchi shelf in
794 the late summer to early fall when waters are more stratified, phytoplankton concentrations are
795 greatly reduced, with blooms occurring only when episodic mixing and/or storm events bring
796 nutrients to the upper water column (e.g. Pickart et al., 2011; Ardyna et al., 2014).
797 A key aspect of this conceptual model is the flow of high-nutrient WW across the shelf that
798 both initiates and sustains phytoplankton blooms in the Chukchi Sea. Given that WW forms
799 locally on the shelf in polynyas and leads during the winter, this implies that blooms in surface
800 waters under melt ponded sea ice are likely widespread across the Chukchi shelf in the spring
801 and early summer. Our observations indicate, however, that phytoplankton blooms along the
802 nutrient-rich WW pathways are extended for longer duration than in adjacent waters, with total
803 bloom duration and the magnitude of primary production related to the residence time and
804 vertical extent of WW flow. Considering that the timing of bloom initiation in the Arctic may be
805 shifting to earlier in the season with a warming climate (Kahru et al., 2010; Arrigo et al., 2012),
806 the role of WW in extending blooms may be particularly important to upper trophic level
807 organisms that rely on the consumption of phytoplankton. Similarly, we have shown that WW

808 flowing through the northeastern Chukchi Sea in the summer en route to Barrow Canyon is
809 characterized by extremely high concentrations of phytoplankton cells that likely sink and
810 provide an important and continuous food source for the rich benthic community in this
811 biological 'hotspot' region. This work furthers our understanding of the hydrographic controls
812 on the timing, magnitude, and dynamics of phytoplankton blooms in the Chukchi Sea.
813
814 **Acknowledgements**
815 This material is based upon work supported by the National Aeronautic and Space
816 Administration (NASA) under Grant No. NNX10AF42G and the National Science Foundation
817 Graduate Research Fellowship under Grant No. DGE-0645962 to K.E. Lowry. The authors
818 would like to acknowledge the scientists, captain, and crew of the USCGC Healy for their efforts
819 during the HLY1001 and HLY1101 missions that supported the collection of field data.
820 Additionally, we would like to thank Carolina Nobre for her efforts that improved the
821 visualization of multiple figures presented in this manuscript.

References

Ardyna, M., Babin, M., Gosselin, M., Devred, E., Bélanger, S., Matsuoka, A., Tremblay, J.É., 2013. Parameterization of vertical chlorophyll a in the Arctic Ocean: impact of the subsurface chlorophyll maximum on regional, seasonal and annual primary production estimates. Biogeosciences 10, 4383–4404. doi:10.5194/bg-10-4383-2013

Ardyna, M., Babin, M., Gosselin, M., Devred, E., Rainville, L., Tremblay, J.-E., 2014. Recent Arctic Ocean sea ice loss triggers novel fall phytoplankton blooms. Geophys. Res. Lett. 41, 6207–6212. doi:10.1002/2014GL061047

Armstrong, F., Stearns, C.R., Strickland, J., 1967. The measurement of upwelling and subsequent biological process by means of the Technicon Autoanalyzer® and associated equipment. Deep-Sea Res. 14, 381–389. doi:10.1016/0011- 7471(67)90082-4

Arrigo, K.R., Perovich, D.K., Pickart, R.S., Brown, Z.W., van Dijken, G.L., Lowry, K.E., Mills, M.M., Palmer, M.A., Balch, W.M., Bates, N.R., Benitez-Nelson, C.R., Brownlee, E., Frey, K.E., Laney, S.R., Mathis, J., Matsuoka, A., Mitchell, B.G., Moore, G.W.K., Reynolds, R.A., Sosik, H.M., Swift, J.H., 2014. Phytoplankton blooms beneath the sea ice in the Chukchi Sea. Deep-Sea Res. 105, 1–16. doi:10.1016/j.dsr2.2014.03.018

Arrigo, K.R., Perovich, D.K., Pickart, R.S., Brown, Z.W., Van Dijken, G.L., Lowry, K., Mills, M.M., Palmer, M.A., Balch, W.M., Bahr, F., Bates, N.R., Benitez-Nelson, C., Bowler, B., Brownlee, E., Ehn, J.K., Frey, K.E., Garley, R., Laney, S.R., Lubelczyk, L., Mathis, J., Matsuoka, A., Mitchell, B.G., Moore, G.W.K., Ortega-Retuerta, E., Pal, S., Polashenski, C.M., Reynolds, R.A., Schieber, B., Sosik, H.M., Stephens, M., Swift, J.H., 2012. Massive Phytoplankton Blooms Under Arctic Sea Ice. Science 336, 1408–1408. doi:10.1126/science.1215065

Arrigo, K.R., Van Dijken, G.L., 2011. Secular trends in Arctic Ocean net primary production. J. Geophys. Res. 116, C09011.

Bates, N.R., Best, M.H.P., Hansell, D.A., 2005. Spatio-temporal distribution of dissolved inorganic carbon and net community production in the Chukchi and Beaufort Seas. Deep-Sea Res. Part II 52, 3303–3323.

Bates, N.R., Cai, W.J., Mathis, J.T., 2011. The ocean carbon cycle in the western Arctic Ocean: Distributions and air-sea fluxes of carbon dioxide. Oceanography 24, 186–201. doi:10.5670/oceanog.2011.71

Brown, Z.W., Casciotti, K.L., Pickart, R.S., Swift, J.H., Arrigo, K.R., 2015. Aspects of the Marine Nitrogen Cycle of the Chukchi Sea shelf and Canada Basin. Deep-Sea Res. Part II, this issue.

Brown, Z.W., Lowry, K.E., Palmer, M.A., Van Dijken, G.L., Mills, M.M., Pickart, R.S., Arrigo, K.R., 2015. Characterizing the Subsurface Chlorophyll a Maximum in the Chukchi Sea. Deep-Sea Res. Part II, this issue.

Campbell, R.G., Sherr, E.B., Ashjian, C.J., Plourde, S., Sherr, B.F., Hill, V., Stockwell, D.A., 2009. Mesozooplankton prey preference and grazing impact in the western Arctic Ocean. Deep-Sea Res. Part II 56, 1274–1289. doi:10.1016/j.dsr2.2008.10.027

Carmack, E., Wassmann, P., 2006. Food webs and physical–biological coupling on pan-Arctic shelves: Unifying concepts and comprehensive perspectives. Prog. Oceanogr. 71, 446–477. doi:10.1016/j.pocean.2006.10.004

866 Cavalieri, D.J., Martin, S., 1994. The contribution of Alaskan, Siberian, and Canadian coastal
867 polynyas to the cold halocline layer of the Arctic Ocean. J. Geophys. Res. 99, 18343–
868 18362. doi:10.1029/94JC01169
869 Coachman, L.K., Aagaard, K., Tripp, R.B., 1975. Bering Strait: The Regional Physical
870 Oceanography. University of Washington Press, Seattle, Washington.
871 Codispoti, L.A., Flagg, C., Kelly, V., Swift, J.H., 2005. Hydrographic conditions during the 2002
872 SBI process experiments. Deep-Sea Res. Part II 52, 3199–3226.
873 Codispoti, L.A., Kelly, V., Thessen, A., Matrai, P., Suttles, S., Hill, V., Steele, M., Light, B.,
874 2013. Synthesis of primary production in the Arctic Ocean: III. Nitrate and phosphate based
875 estimates of net community production. Prog. Oceanogr. 1–25.
876 doi:10.1016/j.pocean.2012.11.006
877 Cooper, L.W., Whitledge, T.E., Grebmeier, J.M., Weingartner, T., 1997. The nutrient, salinity,
878 and stable oxygen isotope composition of Bering and Chukchi Seas waters in and near the
879 Bering Strait. J. Geophys. Res. 102, 12563–12573.
880 Cota, G.F., Pomeroy, L.R., Harrison, W.G., Jones, E.P., Peters, F., Sheldon, W.M., Weingartner,
881 T.R., 1996. Nutrients, primary production and microbial heterotrophy in the southeastern
882 Chukchi Sea: Arctic summer nutrient depletion and heterotrophy. Mar. Ecol. Prog. Ser. 135,
883 247–258.
884 Cullen, J.J., Davis, R.F., 2003. The blank can make a big difference in oceanographic
885 measurements. Limnol. Oceanogr. Bull. 12, 29–35.
886 Dunton, K.H., Goodall, J.L., Schonberg, S.V., Grebmeier, J.M., Maidment, D.R., 2005. Multi-
887 decadal synthesis of benthic–pelagic coupling in the western arctic: Role of cross-shelf
888 advective processes. Deep-Sea Res. Part II 52, 3462–3477.
889 Frey, K.E., Perovich, D.K., Light, B., 2011. The spatial distribution of solar radiation under a
890 melting Arctic sea ice cover. Geophys. Res. Lett. 38, L22501.
891 Gong, D. and R.S. Pickart, 2012. Observations of circulation and water mass transformation in
892 eastern Chukchi Sea. Eos Trans. AGU, abstract 10755.
893 Gong, D., Pickart, R.S., this issue. Summertime Circulation in the Eastern Chukchi Sea. Deep-
894 Sea Res. Part II.
895 Grebmeier, J.M., 2012. Shifting Patterns of Life in the Pacific Arctic and Sub-Arctic Seas. Annu.
896 Rev. Marine. Sci. 4, 63–78. doi:10.1146/annurev-marine-120710-100926
897 Grebmeier, J.M., Cooper, L.W., Feder, H.M., Sirenko, B.I., 2006. Ecosystem dynamics of the
898 Pacific-influenced Northern Bering and Chukchi Seas in the Amerasian Arctic. Prog.
899 Oceanogr. 71, 331–361. doi:10.1016/j.pocean.2006.10.001
900 Hansell, D.A., Whitledge, T.E., Goering, J.J., 1993. Patterns of nitrate utilization and new
901 production over the Bering- Chukchi shelf. Cont. Shelf Res. 13, 601–627.
902 Holm-Hansen, O., Lorenzen, C.J., Holmes, R.W., Strickland, J.D.H., 1965. Fluorometric
903 Determination of Chlorophyll. ICES Journal of Marine Science 30, 3–15.
904 doi:10.1093/icesjms/30.1.3
905 Itoh, M., Shimada, K., Kamoshida, T., McLaughlin, F., Carmack, E., Nishino, S., 2012.
906 Interannual variability of Pacific Winter Water inflow through Barrow Canyon from 2000 to
907 2006. J Oceanogr 68, 575–592.
908 Itoh, M., R.S. Pickart, T. Kikuchi, Y. Fukamachi, K.I. Ohshima, D. Simizu, K.R. Arrigo, S.
909 Vagle, J. He, C. Ashjian, J.T. Mathis, and C. Nobre. Water properties, heat and volume
910 fluxes of Pacific water in Barrow Canyon during summer 2010. Deep-Sea Research,
911 submitted.

912 Iwamoto, K., Ohshima, K.I., Tamura, T., 2014. Improved mapping of sea ice production in the
913 Arctic Ocean using AMSR-E thin ice thickness algorithm. J. Geophys. Res. Oceans 119,
914 3574–3594. doi:10.1002/2013JC009749
915 Jakobsson, M., 2002. Hypsometry and volume of the Arctic Ocean and its constituent seas.
916 Geochem. Geophys. Geosyst. 3, 1–18. doi:10.1029/2001GC000302
917 Jakobsson, M., Grantz, A., Kristoffersen, Y., Macnab, R., 2004. The Arctic Ocean: boundary
918 conditions and background information. In: Stein, R., Macdonald, R.W. (Eds.), The Organic
919 Carbon Cycle in the Arctic Ocean. Springer, New York, pp. 1–5.
920 Kahru, M., Brotas, V., Manzano-Sarabia, M., Mitchell, B.G., 2010. Are phytoplankton blooms
921 occurring earlier in the Arctic? Global Change Biology 17, 1733–1739. doi:10.1111/j.1365-
922 2486.2010.02312.x
923 Kolber, Z.S., Prášil, O., Falkowski, P.G., 1998. Measurements of variable chlorophyll
924 fluorescence using fast repetition rate techniques: defining methodology and experimental
925 protocols. Biochimica et Biophysica Acta (BBA) - Bioenergetics 1367, 88–106.
926 doi:10.1016/S0005-2728(98)00135-2
927 Kwok, R., Rothrock, D.A., 2009. Decline in Arctic sea ice thickness from submarine and ICESat
928 records: 1958–2008. Geophys. Res. Lett. 36.
929 Lee, S.H., Whitledge, T.E., Kang, S.-H., 2007. Recent carbon and nitrogen uptake rates of
930 phytoplankton in Bering Strait and the Chukchi Sea. Cont. Shelf Res. 27, 2231–2249.
931 Loeng, H., Brander, K., Carmack, E., Denisenko, S., Drinkwater, K., Hansen, B., Kovacs, K.,
932 Livingston, P., McLaughlin, F., Sakshaug, E., 2005. Marine Systems, in: Arctic Climate
933 Impact Assessment. Cambridge University Press, Cambridge, UK, pp. 453–538.
934 Lowry, K., Van Dijken, G.L., Arrigo, K.R., 2014. Evidence of under-ice phytoplankton blooms
935 in the Chukchi Sea from 1998 to 2012. Deep-Sea Res. Part II 105, 105–117.
936 doi:10.1016/j.dsr2.2014.03.013
937 Martin, J., Tremblay, J.É., Gagnon, J., Tremblay, G., Lapoussière, A., Jose, C., Poulin, M.,
938 Gosselin, M., Gratton, Y., Michel, C., 2010. Prevalence, structure and properties of
939 subsurface chlorophyll maxima in Canadian Arctic waters. Mar. Ecol. Prog. Ser. 412, 69–84.
940 doi:10.3354/meps08666
941 Maslanik, J., Stroeve, J., Fowler, C., Emery, W., 2011. Distribution and trends in Arctic sea ice
942 age through spring 2011. Geophys. Res. Lett. 38, L13502.
943 Mills, M.M., Brown, Z.W., Lowry, K., Van Dijken, G.L., Becker, S., Pal, S., Benitez-Nelson, C.,
944 Strong, A., Arrigo, K.R., 2015. Impacts of low phytoplankton NO3-:PO43- utilization ratios
945 over the Chukchi Shelf, Arctic Ocean. Deep-Sea Res. Part II, this issue.
946 Muench, R.D., Schumacher, J.D., Salo, S.A., 1988. Winter currents and hydrographic conditions
947 on the northern central Bering Sea shelf. J. Geophys. Res. 93, 516–526.
948 doi:10.1029/JC093iC01p00516.
949 Overland, J.E., Roach, A.T., 1987. Northward flow in the Bering and Chukchi seas. J. Geophys.
950 Res. 92, 7097–7105. doi:10.1029/JC092iC07p07097
951 Palmer, M.A., Saenz, B.T., Arrigo, K.R., 2014. Impacts of sea ice retreat, thinning, and melt-
952 pond proliferation on the summer phytoplankton bloom in the Chukchi Sea, Arctic Ocean.
953 Deep-Sea Res. Part II 105, 85–104.
954 Pickart, R. S., Mao, C., Bahr, F. Winter water in the Chukchi Sea: A revised circulation scheme.
955 Deep-Sea Res. Part II, submitted.
956 Pickart, R.S., Pratt, L.J., Torres, D.J., Whitledge, T.E., Proshutinsky, A.Y., Aagaard, K., Agnew,
957 T.A., Moore, G., Dail, H.J., 2010. Evolution and dynamics of the flow through Herald

Canyon in the western Chukchi Sea. Deep-Sea Res. Part II 57, 5–26.
Pickart, R.S., Spall, M.A., Mathis, J.T., 2013. Dynamics of upwelling in the Alaskan Beaufort Sea and associated shelf– basin fluxes. Deep-Sea Res. I 76, 35–51.
Pickart, R.S., Spall, M.A., Moore, G.W.K., Weingartner, T.J., Woodgate, R.A., Aagaard, K., Shimada, K., 2011. Upwelling in the Alaskan Beaufort Sea: Atmospheric forcing and local versus non-local response. Prog. Oceanogr. 88, 78–100. doi:10.1016/j.pocean.2010.11.005
Pickart, R.S., Weingartner, T.J., Pratt, L.J., Zimmermann, S., Torres, D.J., 2005. Flow of winter-transformed Pacific water into the Western Arctic. Deep-Sea Res. Part II 52, 3175–3198. doi:10.1016/j.dsr2.2005.10.009
Polashenski, C.M., Perovich, D., Courville, Z., 2012. The mechanisms of sea ice melt pond formation and evolution. J. Geophys. Res. 117, C01001. doi:10.1029/2011JC007231
Schlitzer, R., 2012. Ocean Data View. http://odv.awi.de.
Serreze, M.C., Holland, M.M., Stroeve, J., 2007. Perspectives on the Arctic's shrinking sea-ice cover. Science 315, 1533– 1536.
Sherr, E.B., Sherr, B.F., Hartz, A.J., 2009. Microzooplankton grazing impact in the Western Arctic Ocean. Deep-Sea Res. Part II 56, 1264–1273.
Spall, M.A., Pickart, R.S., Brugler, E.T., Moore, G., Thomas, L., Arrigo, K.R., 2014. Role of shelfbreak upwelling in the formation of a massive under-ice bloom in the Chukchi Sea. Deep-Sea Res. 105, 17–29. doi:10.1016/j.dsr2.2014.03.017
Stroeve, J.C., Serreze, M.C., Holland, M.M., Kay, J.E., Malanik, J., Barrett, A.P., 2011. The Arctic's rapidly shrinking sea ice cover: a research synthesis. Clim. Change 110, 1005–1027. doi:10.1007/s10584-011-0101-1
Tremblay, J.-E., Simpson, K., Martin, J., Miller, L., Gratton, Y., Barber, D.G., Price, N.M., 2008. Vertical stability and the annual dynamics of nutrients and chlorophyll fluorescence in the coastal, southeast Beaufort Sea. J. Geophys. Res. 113, C07S90. doi:10.1029/2007JC004547
Tremblay, J.E., Michel, C., Hobson, K.A., Gosselin, M., Price, N.M., 2006. Bloom dynamics in early opening waters of the Arctic Ocean. Limnol. Oceangr. 900–912.
Walsh, J.J., McRoy, C.P., Coachman, L.K., Goering, J.J., Nihoul, J.J., Whitledge, T.E., Blackburn, T.H., Parker, P.L., Wirick, C.D., Shuert, P.G., Grebmeier, J.M., Springer, A.M., Tripp, R.D., Hansell, D.A., Djenidi, S., Deleersnijder, E., Henriksen, K., Lund, B.A., Andersen, P., Mullerkarger, F.E., Dean, K., 1989. Carbon and Nitrogen Cycling within the Bering Chukchi Seas - Source Regions for Organic-Matter Effecting Aou Demands of the Arctic-Ocean. Prog. Oceanogr. 22, 277–359.
Weingartner, T., Aagaard, K., Woodgate, R., Danielson, S., Sasaki, Y., Cavalieri, D., 2005. Circulation on the north central Chukchi Sea shelf. Deep-Sea Res. Part II 52, 3150–3174.
Weingartner, T.J., Cavalieri, D.J., Aagaard, K., Sasaki, Y., 1998. Circulation, dense water formation, and outflow on the northeast Chukchi shelf. J. Geophys. Res. 103, 7647–7661.
Winsor, P., Chapman, D.C., 2002. Distribution and interannual variability of dense water production from coastal polynyas on the Chukchi Shelf. J. Geophys. Res. 107, 3079. doi:10.1029/2001JC000984
Woodgate, R.A., Aagaard, K., 2005a. Monthly temperature, salinity, and transport variability of the Bering Strait through flow. Geophys. Res. Lett. 32, L04601. doi:10.1029/2004GL021880
Woodgate, R.A., Aagaard, K., 2005b. Revising the Bering Strait freshwater flux into the Arctic Ocean. Geophys. Res. Lett. 32, L02602. doi:10.1029/2004GL021747
Woodgate, R.A., Aagaard, K., Swift, J.H., Falkner, K.K., Smethie, W.M.J., 2005a. Pacific

ventilation of the Arctic Ocean's lower halocline by upwelling and diapycnal mixing over the continental margin. Geophys. Res. Lett. 32, L18609. doi:10.1029/2005GL023999

Woodgate, R.A., Aagaard, K., Weingartner, T.J., 2005b. A year in the physical oceanography of the Chukchi Sea: Moored measurements from autumn 1990–1991. Deep-Sea Res. Part II 52, 3116–3149.

Woodgate, R.A., Weingartner, T.J., Lindsay, R., 2012. Observed increases in Bering Strait oceanic fluxes from the Pacific to the Arctic from 2001 to 2011 and their impacts on the Arctic Ocean water column. Geophys. Res. Lett. 39, L24603. doi:10.1029/2012GL054092

Zhang, J., Spitz, Y.H., Steele, M., Ashjian, C.J., Campbell, R., Berline, L., Matrai, P., 2010. Modeling the impact of declining sea ice on the Arctic marine planktonic ecosystem. J. Geophys. Res. 115, 1–24.

Figure 1. Map of the northeastern Chukchi Sea illustrating bathymetry, the seven transects sampled as part of our field campaign in 2010-2011 that we focus on in this study, and the main pathway of winter water (WW) as it flowed across the Chukchi shelf during our sampling period (as identified and described in more detail by Pickart et al. (submitted)).

Figure 2. Vertical sections of absolute geostrophic velocity illustrating the speed and direction of currents through transects (**A**) Central Channel, (**B**) Chukchi North, (**C**) Chukchi Slope West, (**D**) Hanna Shoal North, (**E**) Chukchi Slope Center, (**F**) Chukchi Slope East, and (**G**) Hanna Shoal Southeast. Positive values indicate flow into the page, while negative values indicate flow out of the page. Locations where absolute geostrophic velocity equals zero are labeled and sections are overlain by the WW isotherm (θ =-1.6°C; black line).

Figure 3. The Central Channel transect was sampled on 29 June - 1 July 2010 and is displayed here from northwest (left) to southeast (right). (**A-G**) Hydrographic sections of (A) θ, (B) salinity, (C) NO_3^-, (D) DIC, (E) Chl *a*, (F) POC, and (G) O_2 saturation, overlain by σ_θ (kg m^{-3}; thin black lines with labels) and the WW isotherm (θ=-1.6°C; thick black line). Station numbers are below (A) and (B) and black dots represent sampling depths. (**H**) Satellite-based open water duration, indicating the number of days each station was in open water from the time of ice retreat until the date of sampling. Note that this transect is referred to as the Central Slope transect in Gong and Pickart (this issue).

Figure 4. The Chukchi North transect was sampled on 3-5 July 2011 and is displayed here from northwest (left) to southeast (right). (**A-G**) Hydrographic sections of (A) θ, (B) salinity, (C) NO_3^-, (D) DIC, (E) Chl *a*, (F) POC, and (G) O_2 saturation, overlain by σ_θ (kg m^{-3}; thin black lines with labels) and the WW isotherm (θ=-1.6°C; thick black line). Station numbers are below (A) and (B) and black dots represent sampling depths. (**H**) Satellite-based open water duration, indicating the number of days each station was in open water from the time of ice retreat until the date of sampling. Note that because this transect was sampled in a different year than the Central Channel transect (Fig. 3), there are overlapping station numbers between the two transects that refer to different locations.

Figure 5. The Chukchi Slope West transect was sampled on 7-9 July 2011 and is displayed here from northwest (left) to southeast (right). (**A-G**) Hydrographic sections of (A) θ, (B) salinity, (C) NO_3^-, (D) DIC, (E) Chl *a*, (F) POC, and (G) O_2 saturation, overlain by σ_θ (kg m^{-3}; thin black lines with labels) and the WW isotherm (θ=-1.6°C; thick black line). Station numbers are below (A) and (B) and black dots represent sampling depths. (**H**) Satellite-based open water duration, indicating the number of days each station was in open water from the time of ice retreat until the date of sampling.

Figure 6. Hydrographic section of Fv:Fm for three stations in the Chukchi Slope West transect. The section is overlain by the WW isotherm (θ =-1.6°C; thick black line), consistent with biogeochemical properties displayed in Fig. 5A-G. Station numbers are listed above the plot.

Figure 7. The Hanna Shoal North transect was sampled on 9-10 July 2011 and is displayed here from northwest (left) to southeast (right). (**A-G**) Hydrographic sections of (A) θ, (B) salinity, (C) NO_3^-, (D) DIC, (E) Chl *a*, (F) POC, and (G) O_2 saturation, overlain by σ_θ (kg m^{-3}; thin black lines with labels) and the WW isotherm (θ=-1.6°C; thick black line). Station numbers are below (A) and (B) and black dots represent sampling depths. (**H**) Satellite-based open water duration, indicating the number of days each station was in open water from the time of ice retreat until the date of sampling.

Figure 8. The Chukchi Slope Center transect was sampled on 10-12 July 2011 and is displayed here from northeast (left) to southwest (right). (**A-G**) Hydrographic sections of (A) θ, (B) salinity, (C) NO_3^-, (D) DIC, (E) Chl *a*, (F) POC, and (G) O_2 saturation, overlain by σ_θ (kg m^{-3}; thin black lines with labels) and the WW isotherm (θ=-1.6°C; thick black line). Station numbers are below (A) and (B) and black dots represent sampling depths. (**H**) Satellite-based open water duration, indicating the number of days each station was in open water from the time of ice retreat until the date of sampling.

Figure 9. The Chukchi Slope East transect was sampled on 14-16 July 2011 and is displayed here from northeast (left) to southwest (right). (**A-G**) Hydrographic sections of (A) θ, (B)

1070 salinity, (C) NO_3^-, (D) DIC, (E) Chl *a*, (F) POC, and (G) O_2 saturation, overlain by σ_θ (kg
1071 m^{-3}; thin black lines with labels) and the WW isotherm (θ=-1.6°C; thick black line).
1072 Station numbers are below (A) and (B) and black dots represent sampling depths. (**H**)
1073 Satellite-based open water duration, indicating the number of days each station was in open
1074 water from the time of ice retreat until the date of sampling.
1075 **Figure 10.** The Hanna Shoal Southeast transect was sampled on 16 July 2011 and is displayed
1076 here from southeast (left) to northwest (right). (**A-G**) Hydrographic sections of (A) θ, (B)
1077 salinity, (C) NO_3^-, (D) DIC, (E) Chl *a*, (F) POC, and (G) O_2 saturation, overlain by σ_θ (kg
1078 m^{-3}; thin black lines with labels) and the WW isotherm (θ=-1.6°C; thick black line).
1079 Station numbers are below (A) and (B) and black dots represent sampling depths. (**H**)
1080 Satellite-based open water duration, indicating the number of days each station was in open
1081 water from the time of ice retreat until the date of sampling.
1082 **Figure 11.** Plots of θ versus NO_3^- for all bottle samples in the upper 60 m from each transect:
1083 (**A**) Central Channel (2010), (**B**) Chukchi North, (**C**) Chukchi Slope West, (**D**) Hanna
1084 Shoal North, (**E**) Chukchi Slope Center, (**F**) Chukchi Slope East, (**G**) Hanna Shoal
1085 Southeast, (**H**) Chukchi North (2010), and (**I**) Hanna Shoal North (2010).
1086 **Figure 12.** Mean depth-integrated Chl *a* values with standard error bars for all winter water
1087 (WW) and non-winter water (non-WW) stations (n=100 and n=202, respectively). Water
1088 column mean chlorophyll *a* concentrations ($\bar{x}$) and standard deviations (±SD) are also
1089 presented for WW and non-WW stations. Note that these values represent all ICESCAPE
1090 data collected in 2010 and 2011 and are not limited to shelf waters or the seven transects
1091 that we focus on in this study.
1092

Table 1. Mean and standard deviation of θ, salinity, σ_θ, NO_3^-, DIC, Chl *a*, POC, and O_2 saturation for all WW (θ ≤ -1.6°C) and non-WW (θ > -1.6°C) samples in the upper 60 m of each transect. Bold WW values indicate statistically significant differences from the respective non-WW values ($p<0.05$).

		θ (°C)	Salinity	σ_θ (kg m^{-3})	NO_3^- (μmol L^{-1})	DIC (μmol L^{-1})	Chl *a* (μg L^{-1})	POC (μmol L^{-1})	O_2 Sat (%)
Central Channel	WW	**-1.68 ± 0.04**	**32.88 ± 0.16**	**26.46 ± 0.13**	**12.0 ± 1.71**	**2203 ± 52**	3.53 ± 3.75	**18.7 ± 12.4**	**90.7 ± 6.8**
	Non-WW	1.00 ± 2.18	32.12 ± 0.73	25.70 ± 0.63	1.85 ± 3.15	2048 ± 101	5.40 ± 8.53	36.3 ± 33.1	114 ± 14.4
Chukchi North	WW	**-1.72 ± 0.05**	**32.88 ± 0.29**	**26.46 ± 0.24**	**12.1 ± 6.27**	**2225 ± 65**	**7.98 ± 9.56**	23.4 ± 17.0	**95.3 ± 10.9**
	Non-WW	0.61 ± 1.54	32.23 ± 0.57	25.83 ± 0.49	1.73 ± 3.76	2049 ± 96	2.35 ± 3.50	19.3 ± 14.2	112 ± 11.7
Chukchi Slope West	WW	**-1.71 ± 0.05**	**32.59 ± 0.42**	**26.23 ± 0.34**	**12.7 ± 6.21**	**2216 ± 77**	**9.18 ± 8.17**	19.7 ± 15.6	**97.9 ± 17.0**
	Non-WW	-0.14 ± 1.48	31.47 ± 0.88	25.25 ± 0.69	1.02 ± 2.57	2003 ± 76	5.33 ± 7.75	31.8 ± 25.6	117 ± 11.6
Hanna Shoal North	WW	**-1.72 ± 0.04**	**32.82 ± 0.26**	**26.41 ± 0.21**	**12.4 ± 5.56**	**2236 ± 48**	**10.4 ± 6.02**	**31.7 ± 12.6**	**93.8 ± 11.5**
	Non-WW	-0.43 ± 1.21	31.25 ± 0.99	25.09 ± 0.80	0.09 ± 0.19	1983 ± 77	1.66 ± 1.36	16.3 ± 6.2	119 ± 8.9
Chukchi Slope Center	WW	**-1.70 ± 0.03**	**32.39 ± 0.21**	**26.07 ± 0.17**	**13.7 ± 3.61**	**2252 ± 16**	**14.2 ± 19.8**	**44.9 ± 55.1**	**88.2 ± 12.6**
	Non-WW	-1.11 ± 0.70	29.77 ± 1.47	23.93 ± 1.19	0.51 ± 1.50	1996 ± 81	0.61 ± 1.58	5.7 ± 7.3	107 ± 7.0
Chukchi Slope East	WW	**-1.70 ± 0.04**	**32.41 ± 0.21**	**26.08 ± 0.17**	**12.5 ± 3.52**	**2236 ± 36**	**10.8 ± 9.51**	**39.4 ± 29.8**	**89.7 ± 13.5**
	Non-WW	-0.82 ± 0.79	30.38 ± 1.58	24.41 ± 1.3	0.90 ± 2.39	1983 ± 159	3.35 ± 6.55	10.3 ± 8.3	108 ± 8.6
Hanna Shoal Southeast	WW	**-1.64 ± 0.03**	**32.39 ± 0.19**	**25.98 ± 0.15**	**9.78 ± 4.45**	**2230 ± 45**	4.60 ± 4.04	17.6 ± 22.9	**85.6 ± 8.2**
	Non-WW	0.23 ± 1.63	31.16 ± 0.79	24.99 ± 0.68	1.22 ± 2.74	2056 ± 90	3.35 ± 6.55	14.1 ± 10.8	105 ± 7.9
All Transects	WW	**-1.71 ± 0.05**	**32.68 ± 0.37**	**26.30 ± 0.30**	**12.3 ± 5.13**	**2222 ± 63**	**8.64 ± 9.75**	**25.0 ± 22.5**	**94.1 ± 13.8**
	Non-WW	-0.21 ± 1.55	31.00 ± 1.49	24.87 ± 1.19	1.13 ± 2.71	2019 ± 107	2.79 ± 5.58	19.2 ± 21.4	110 ± 11.0

Fig. 1

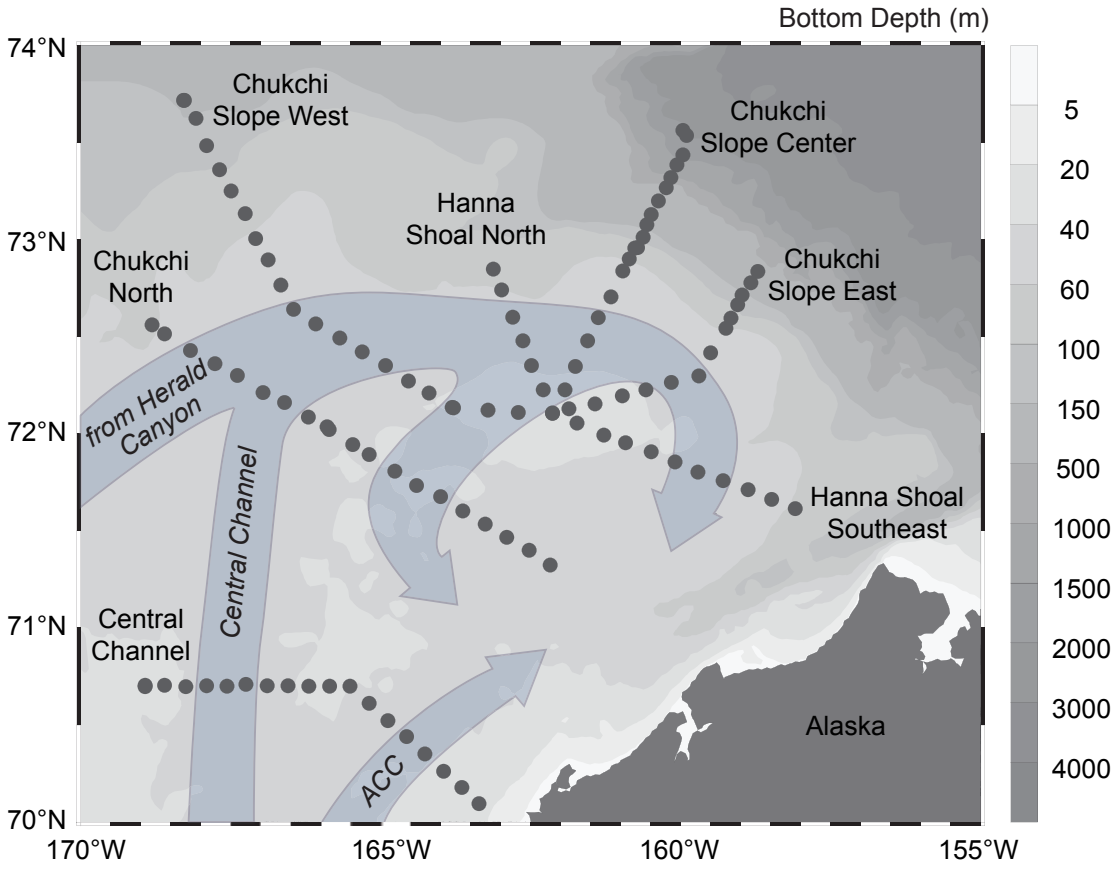
Bottom Depth (m)
74°N
73°N
72°N
71°N
70°N
170°W
165°W
160°W
155°W
Chukchi Slope West
Chukchi Slope Center
Hanna Shoal North
Chukchi North
Chukchi Slope East
from Herald Canyon
Central Channel
Hanna Shoal Southeast
Central Channel
ACC
Alaska
5
20
40
60
100
150
500
1000
1500
2000
3000
4000

Fig. 2

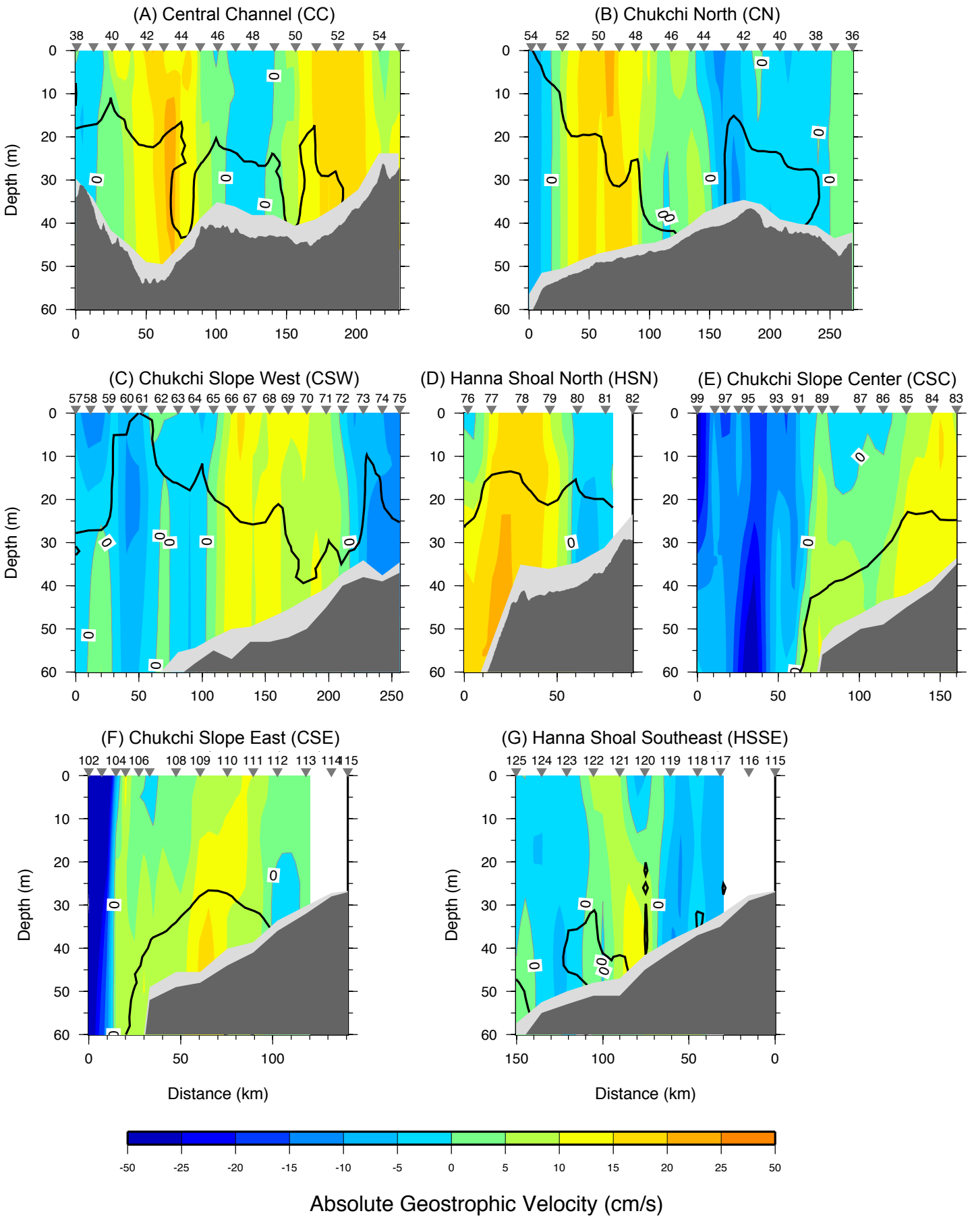
(A) Central Channel (CC)
(B) Chukchi North (CN)
(C) Chukchi Slope West (CSW)
(D) Hanna Shoal North (HSN)
(E) Chukchi Slope Center (CSC)
(F) Chukchi Slope East (CSE)
(G) Hanna Shoal Southeast (HSSE)
Depth (m)
Distance (km)
-50 -25 -20 -15 -10 -5 0 5 10 15 20 25 50
Absolute Geostrophic Velocity (cm/s)

Fig. 3: Central Channel Transect, 2010

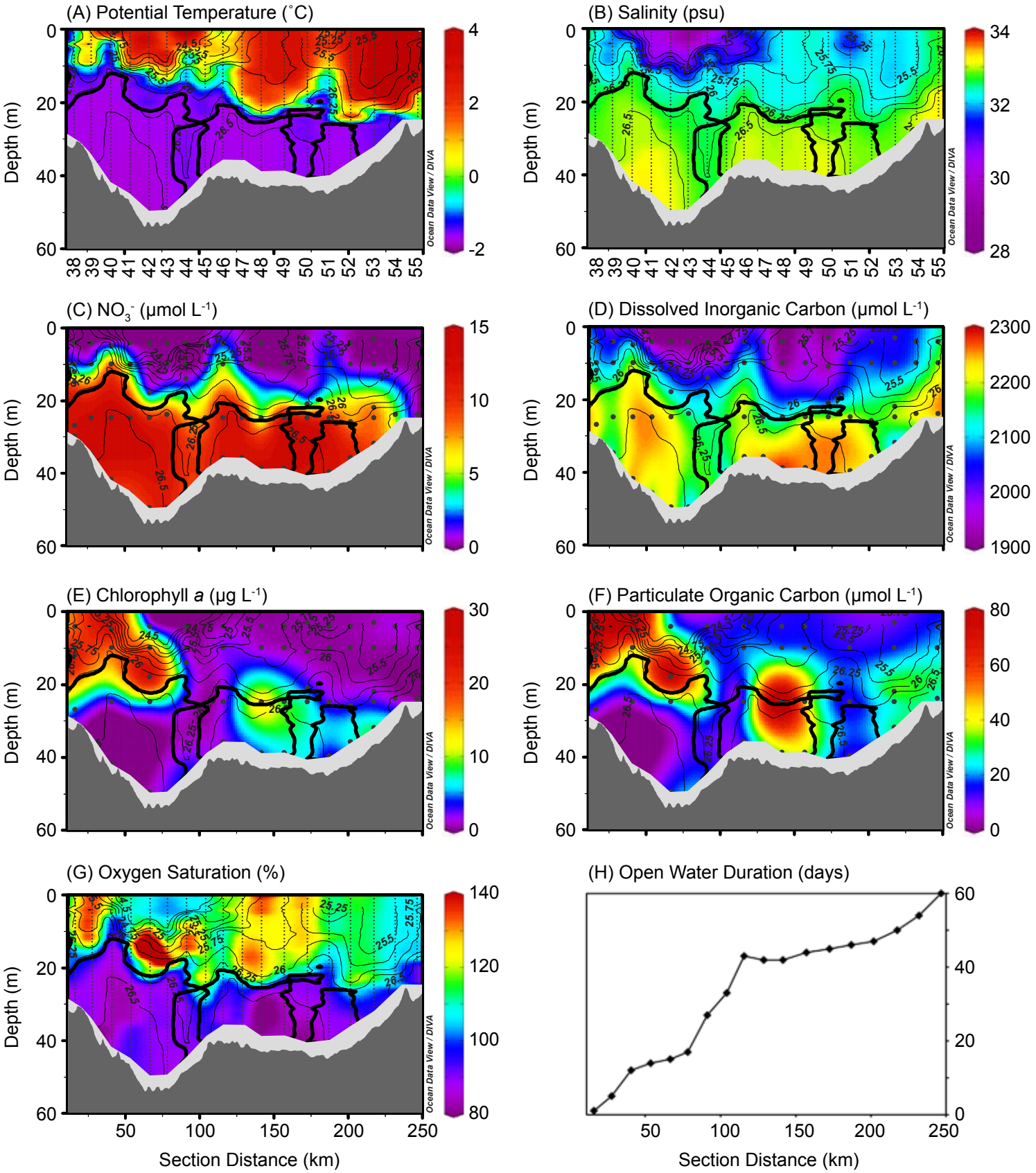

Fig. 4: Chukchi North, 2011

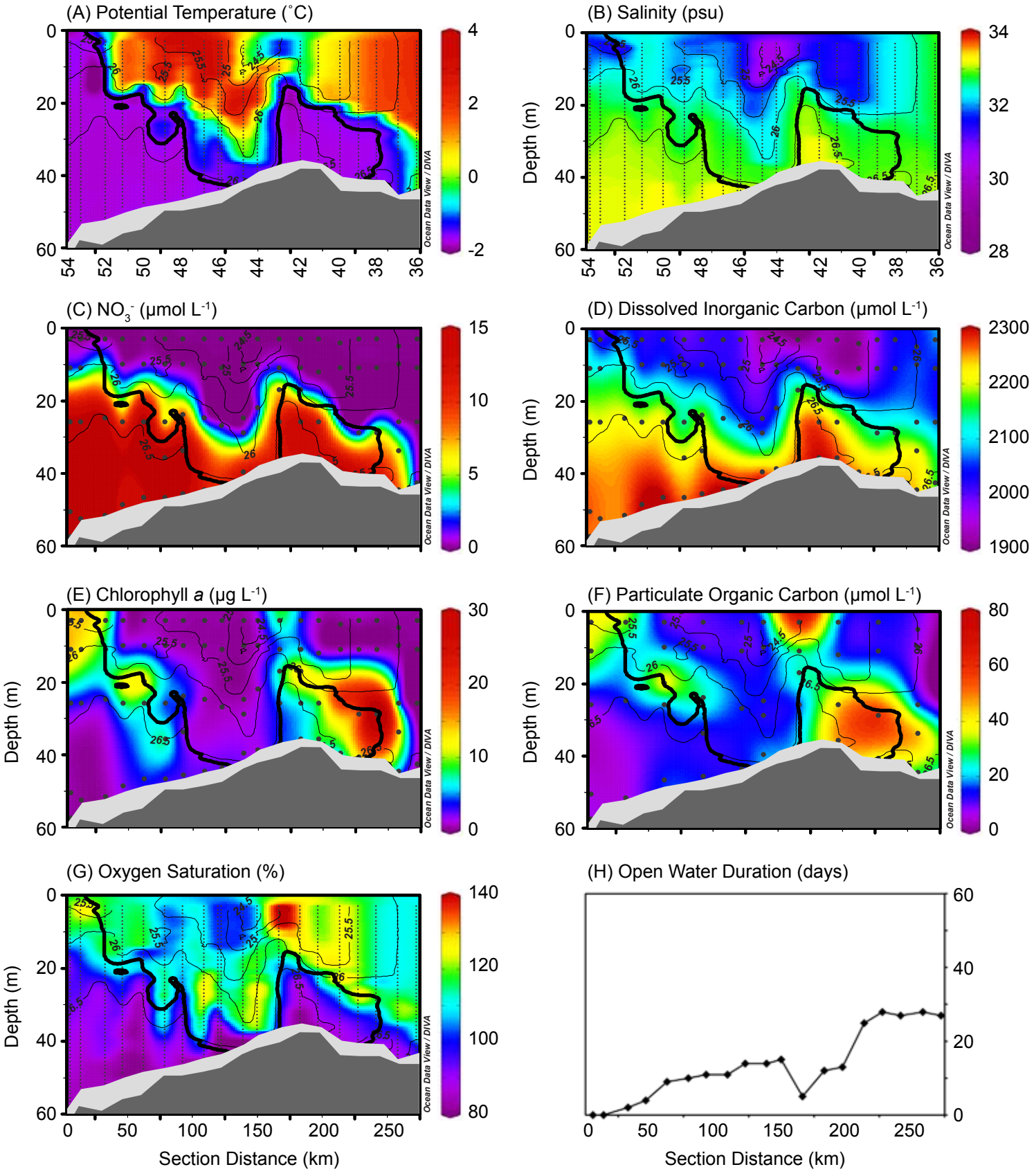

Fig. 5: Chukchi Slope West, 2011

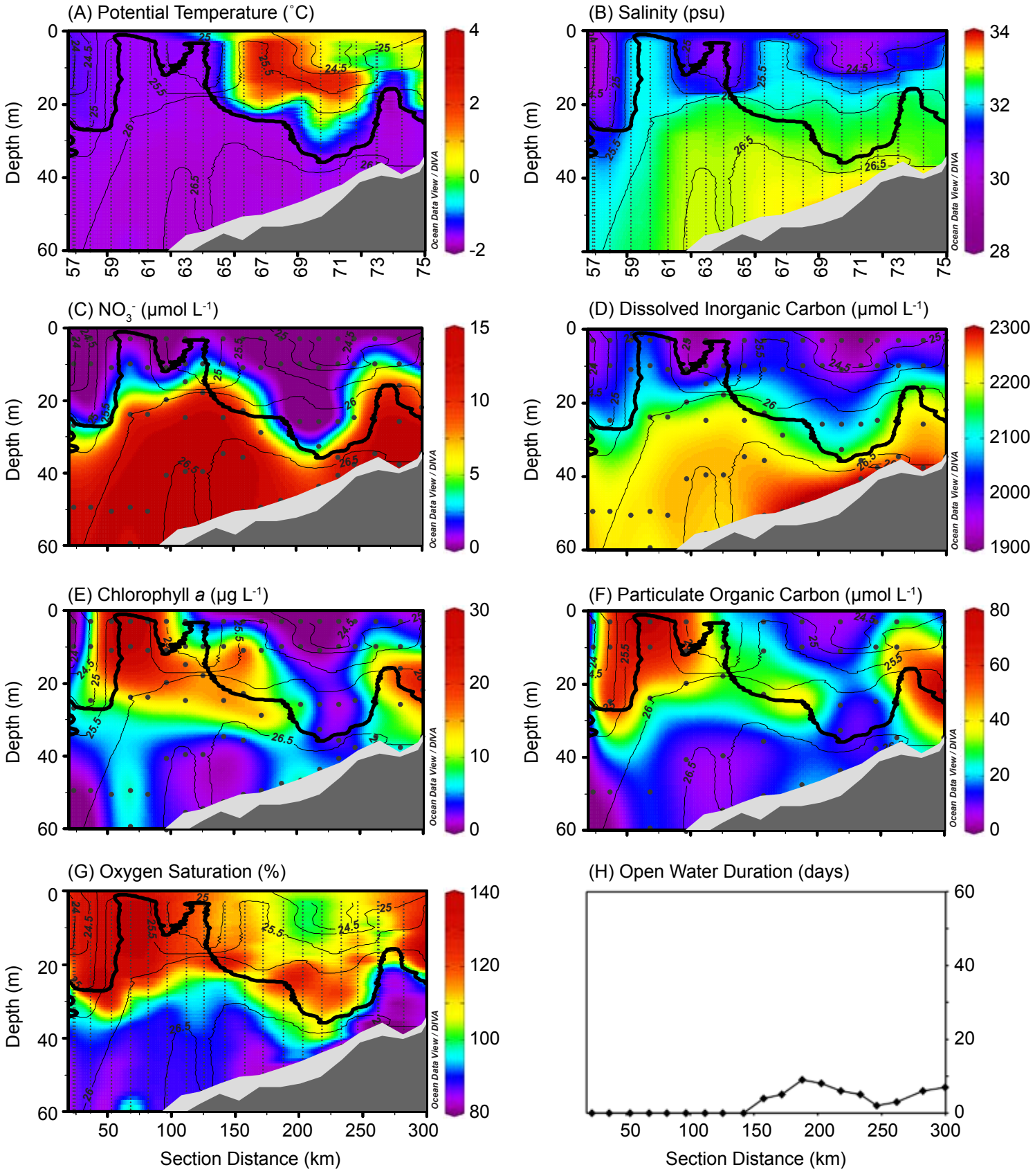

Fig. 6: Fv:Fm for the Chukchi Slope West Transect

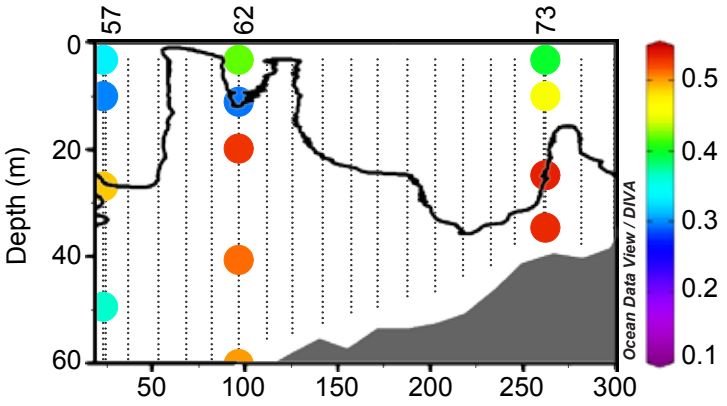

Fig. 7: Hanna Shoal North, 2011

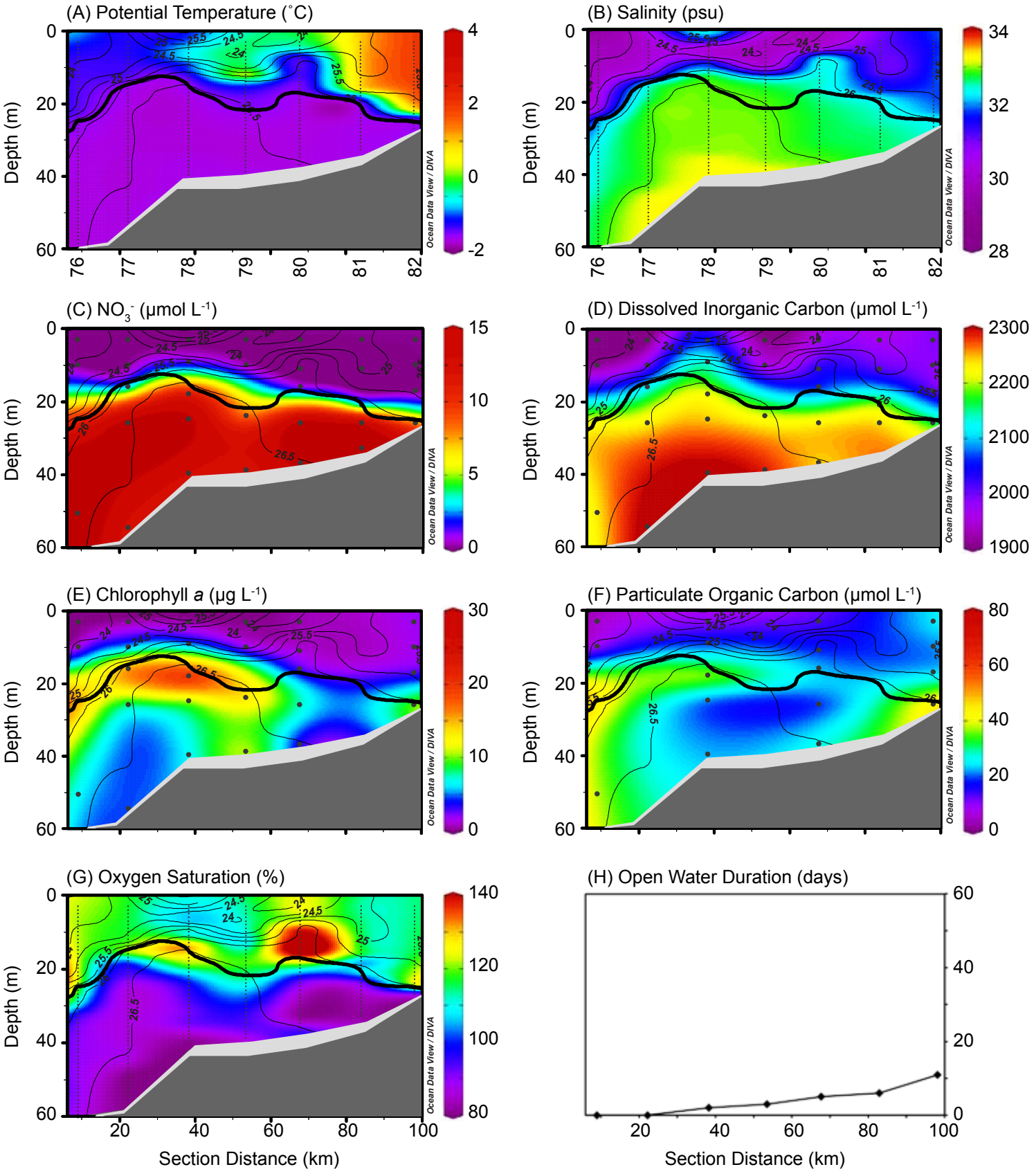

Fig. 8: Chukchi Slope Center, 2011

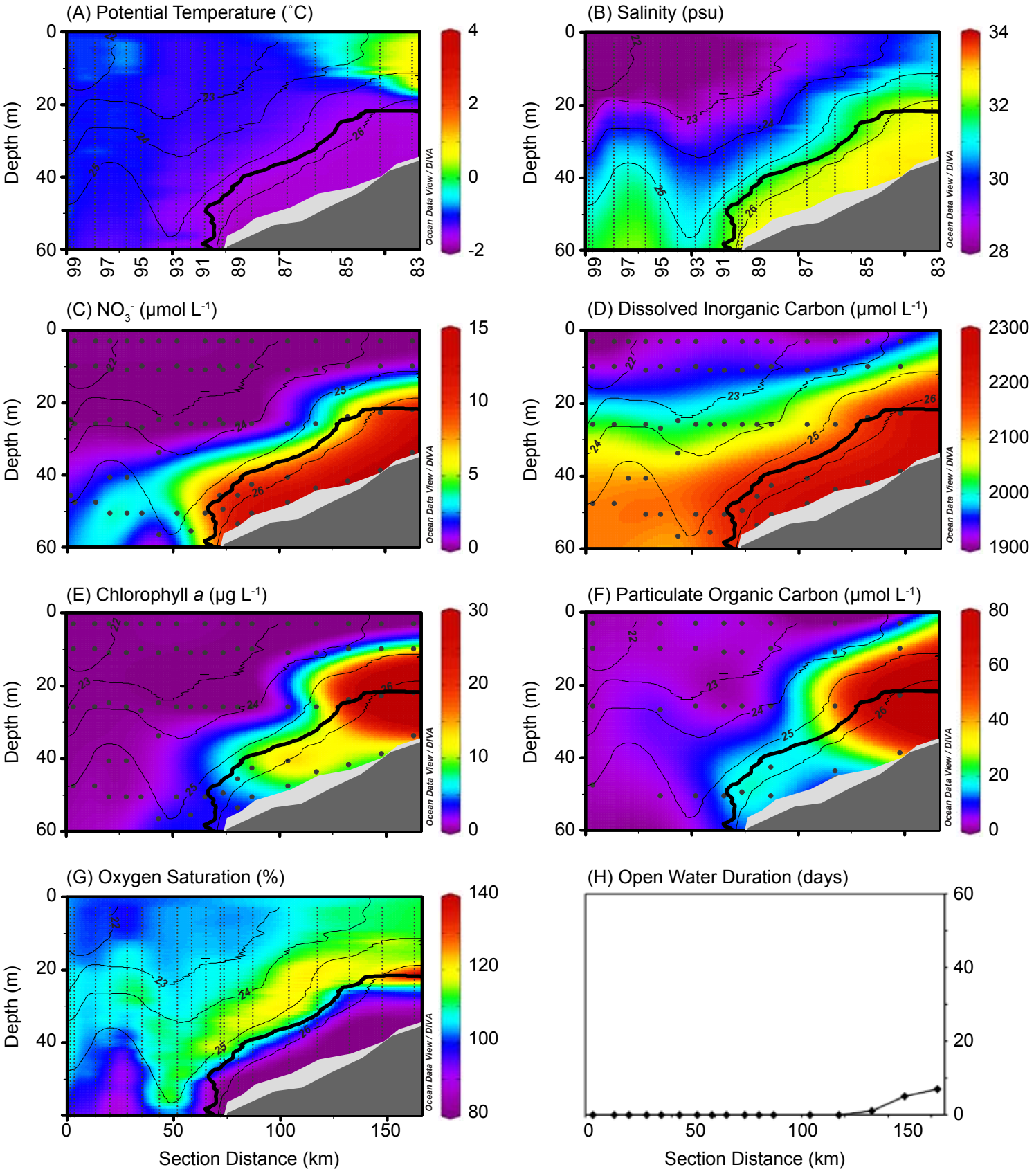

Fig. 9: Chukchi Slope East, 2011

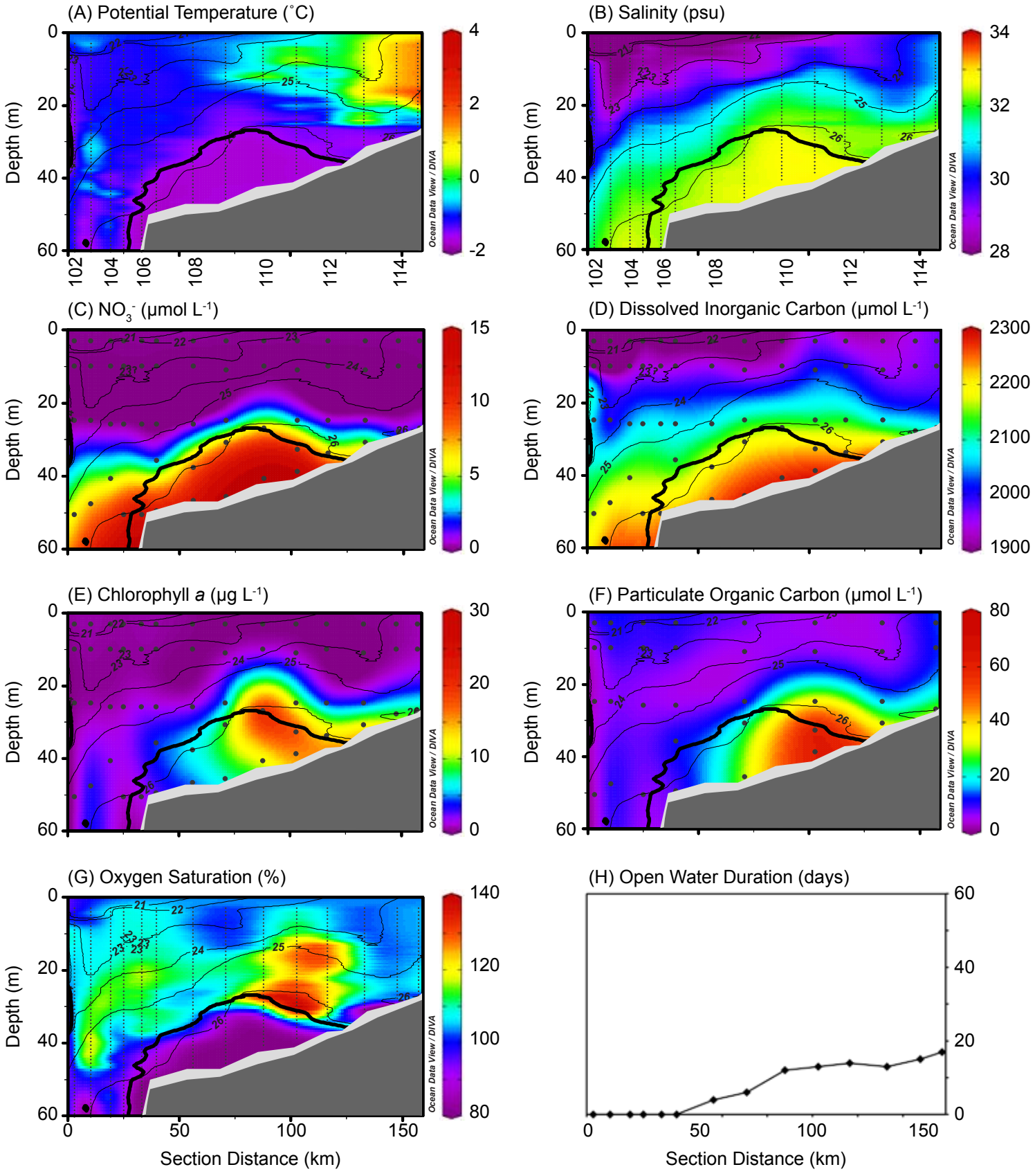

Fig. 10: Hanna Shoal Southeast, 2011

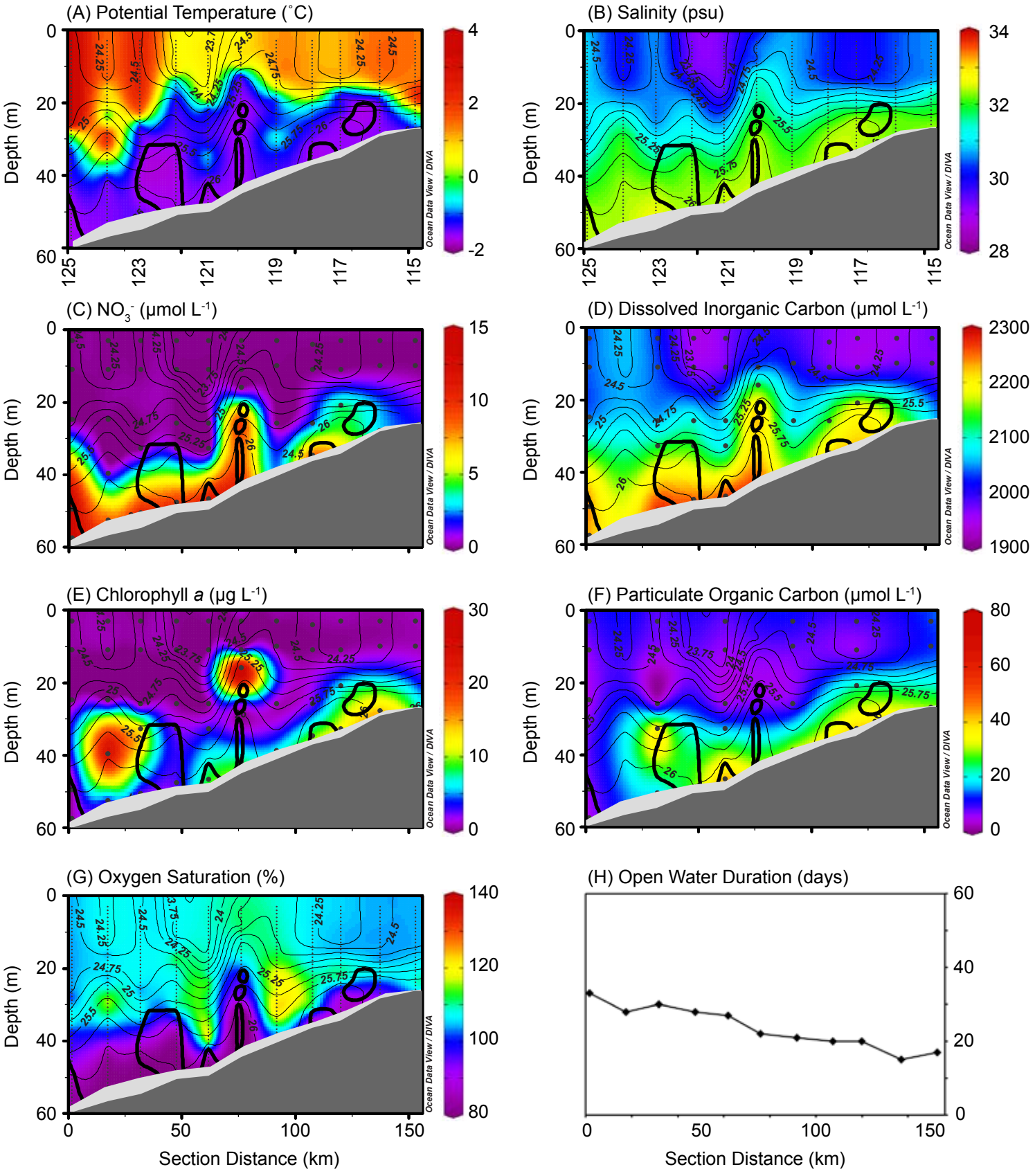

Fig. 11

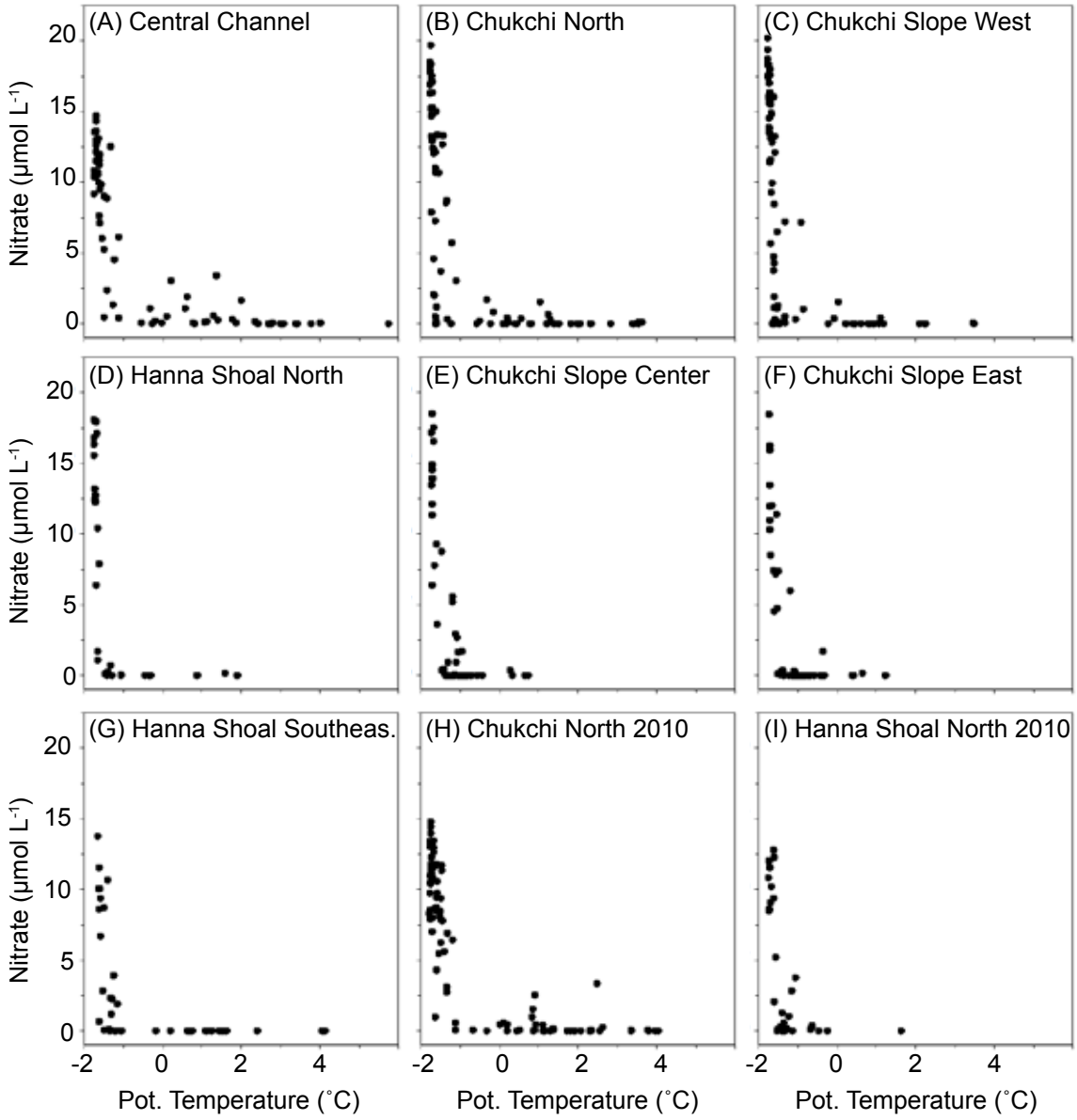
(A) Central Channel
(B) Chukchi North
(C) Chukchi Slope West
(D) Hanna Shoal North
(E) Chukchi Slope Center
(F) Chukchi Slope East
(G) Hanna Shoal Southeas.
(H) Chukchi North 2010
(I) Hanna Shoal North 2010
Nitrate (µmol L-1)
Pot. Temperature (˚C)
0
5
10
15
20
-2
0
2
4

Fig. 12

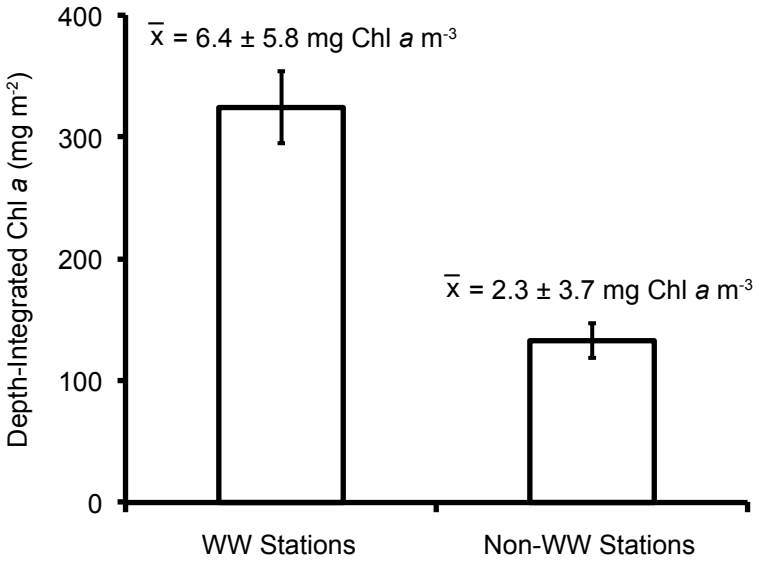
400
300
200
100
0
Depth-Integrated Chl *a* (mg m^{-2})
$\bar{x}$ = 6.4 ± 5.8 mg Chl *a* m^{-3}
$\bar{x}$ = 2.3 ± 3.7 mg Chl *a* m^{-3}
WW Stations
Non-WW Stations